Journal Pre-proofs

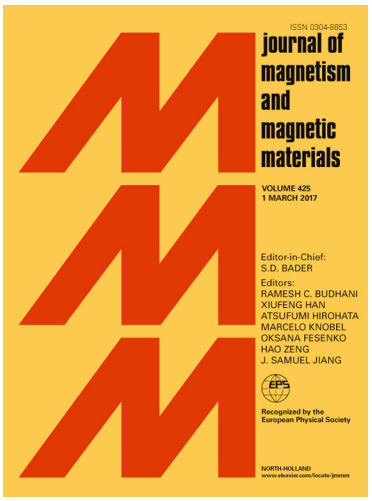

Magnetic hydrogel based shoe insoles for prevention of diabetic foot

Rahul Patwa, Nabanita Saha, Petr Sáha

PII: S0304-8853(20)30228-6
DOI: https://doi.org/10.1016/j.jmmm.2020.167153
Reference: MAGMA 167153

To appear in: *Journal of Magnetism and Magnetic Materials*

Received Date: 27 January 2020
Accepted Date: 14 June 2020

Please cite this article as: R. Patwa, N. Saha, P. Sáha, Magnetic hydrogel based shoe insoles for prevention of diabetic foot, *Journal of Magnetism and Magnetic Materials* (2020), doi: https://doi.org/10.1016/j.jmmm.2020.167153

Magnetic hydrogel based shoe insoles for prevention of diabetic foot

Rahul Patwa[a,*], Nabanita Saha[a,b*], Petr Sáha[a,b]

[a]Centre of Polymer Systems, University Institute, Tomas Bata University in Zlín, Tř. T. Bati 5678, 760 01 Zlín, Czech Republic

[b]University Institute, Nad Ovčírnou 3685, 760 01 Zlín Czech Republic

[*]Correspondence to: N. Saha (Email: nabanita@utb.cz), R. Patwa (Email: patwa@utb.cz)

Highlights

- PVA/CMC hydrogels containing strontium ferrite nanoparticles were synthesized.
- Moist heat treatment method was used to physically crosslink the hydrogels.
- Magnetic fillers improve the mechanical and thermal properties.
- Magnetic hydrogels have high flexibility and film forming ability
- PVA/CMC/MG hydrogels are biodegradable, sweat absorbing, odor-resistant and comfortable as compared to plastic based magnetic diabetic insoles.

Abstract

Currently, plastic/rubber/silicone based shoe inserts are used as preventive approach against diabetic foot which are non-degradable, non-absorbent and contains magnet protrusions, making them highly uncomfortable. These are discarded and thrown away after their service life, causing soil and marine pollution. Thus the objective of this study was to evaluate polyvinyl alcohol/carboxymethyl cellulose (PVA/CMC) based magnetic hydrogels prepared by physical crosslinking as an alternative for diabetic shoe inserts. Hydrogels prepared by moist heat treatment with different concentration of strontium ferrite nanoparticles (MG) are evaluated based on their structural, physico-chemical, morphological, thermal, mechanical, thermo-mechanical, swelling behavior, surface wetting, magnetic and rheological properties. It was observed that incorporation of MG resulted in improvement in overall properties. Infrared spectroscopy revealed strong hydrogen bonding interaction between CMC and PVA. The surface micrographs showed uniform dispersion of MG throughout PVA/CMC matrix. The results showed the improvement in flexibility and tensile strength of the PVA/CMC hydrogels with the incorporation of MG by ~40

and ~20%, respectively. Moreover, the magnetic hydrogels could absorb ~300% moisture of their original weight which is necessary to avoid growth of microbes on skin. Thus, PVA/CMC/MG hydrogels can be considered as a biodegradable alternative for diabetic shoe insoles.

Keywords

Hydrogel; magnetic; diabetes; nanocomposites; nanoparticles

Graphical Abstract

1. Introduction

Diabetes mellitus is a chronic disease where pancreas cannot make enough insulin or body fails to effectively utilize the insulin prepared by it. As per 2017 data, this affects approximately 425 million people worldwide [1, 2]. Diabetes, if not monitored properly leads long-term complications such as diabetic neuropathy (DN) and peripheral vascular disease (PVD) which causes dental, retinal, renal, cardiovascular and foot diseases [3, 4]. PVD is a condition where blood circulation through blood vessels of the limbs is affected due to formation of plaques causing narrowing of blood vessels [5]. Subsequently, reduced blood flow leads to lower blood supply to nerves resulting in oxygen deprivation causing nerve cell death causing loss of sensation and numbness, a situation commonly known as neuropathy [2, 6]. These diabetic complications most severely affect the human foot which due to pressure from body weight and shear from ground and footwear manifests blisters and ulcers making healing time longer than normal often resulting in amputations. An estimated 25% diabetics suffer from wound and ulcer problems furthermore c.a.70% leg amputations occur with people with diabetes [7].

Currently diabetic foot ulcers are treated by glycemic monitoring, debridement of edema, off-loading strategies, surgical revascularization, antibiotic therapies, etc. [8, 9]. In addition, advanced wound therapies such as use of hyperbaric oxygen and stem cell derived allograft are being used readily in some cases [10, 11]. It is noteworthy to mention that except glycemic control, all the above strategies are curative instead of being preventive which is imperative for diabetic foot treatment (DFT) [12]. Magnetotherapy is regarded as a non-invasive and inexpensive

preventive strategy for DFT that can easily be combined with glycemic control and lifestyle changes [13, 14].

Magnetotherapy has existed since the dawn of civilization for treatment of a variety of medical conditions such as inflammation, fractures, skin lesions, etc. [15]. It is based on the phenomenon, that when a conductor (blood vessel in case of the human body) is placed perpendicular to a magnet, the ions present in blood experience a force, thereby dilating the blood vessels and producing heat, this phenomenon is known as Hall Effect [16, 17]. In view of this, application of a magnet underneath the feet can facilitate the blood circulation by causing the ions to move/vibrate thus dilating the blood capillaries which can help to avoid the complications of diabetic foot at a very early stage of diabetes. At present, the market is flooded with many medicated magnetic insoles for diabetic foot treatment [12, 18-20]. Nonetheless, they suffer from a variety of limitations. Firstly, they are made up of non-degradable materials such as treated rubber, ethylene vinyl acetate (EVA), silicone, polyurethane which after their service life are thrown away [21]. Secondly, they contain magnetic beads which mostly protrude outwards creating a lot of discomfort for the person wearing them. Thirdly, the above mentioned materials have a low air permeability and do not absorb moisture which leads to sweat and odor [22]. Hence there is a scope for a better suited material for magnetic insoles.

Among the various available engineering materials, hydrogels can be an ideal material for applications related with interactions with human body such as contact lenses, tissue engineering, sensors, etc., owing to its superior biocompatibility, flexibility, hydrophilicity, insolubility in water and ability to tune their properties as per requirement [23]. Hydrogels are three-dimensional (3D) network structures formed by polymer chain crosslinking through van der Waals forces, hydrogen or covalent bonding [24]. Chemical crosslinking though leads to well-defined shape and better mechanical properties but use chemical crosslinkers and other chemical solvents which are toxic and also reduce the biocompatibility significantly [25, 26]. As a result it is not recommended to use such process for feet with blisters and wounds. Alternatively, physical crosslinking becomes the more suited approach. It can be obtained by use of metallic ions such as Ca^{2+} and Ba^{2+}, crystallization using freeze-thaw method, irradiation, temperature induced, etc. [27-30]. The crystallization method is a time consuming method whereas the irradiation method requires

expensive laboratory setup. Moist heat treatment method is a facile, low-cost, sterile method which can be used for hydrogel production [31, 32].

Recently, use of biopolymers for preparation of hydrogels have aroused interest for the scientific community owing to their low-cost, abundance and environment friendly nature. Most commonly used biopolymers for hydrogels are cellulose, alginate, chitosan, gelatin, carrageenan, polyvinyl alcohol (PVA), carboxymethyl cellulose (CMC), polyvinyl pyrollidone (PVP), etc. They can be used separately or blended in different ratios to produce hydrogels. PVA is a semicrystalline polymer which is biocompatible, biodegradable and chemically stable, it is obtained from polyvinyl acetate by the process of hydrolysis. PVA possesses high flexibility and tensile strength along with hydrophilic hydroxyl sidegroups which allows for functionalization [33]. CMC is a derivative of cellulose and is fully biodegradable, non-toxic, low-cost and semicrystalline material which has excellent film forming ability [34]. However, CMC suffers from small elongation at break making it highly stiff especially in swollen state [35]. Due to its stiffness, CMC is added to hydrogels to improve the moduli. It was found that blending of CMC with PVA results in effective hydrogen affinity membranes with improved properties which can be effectively used for many applications. PVA/CMC hydrogels have been prepared by irradiation, freeze thaw methods, etc. and are found to have exceptional wound dressing material [35-37].

In recent times, a variety of fillers have been incorporated into hydrogels to modify the properties of hydrogels suited for various applications. Fillers such as graphene oxide, bentonite, copper oxide, cobalt oxide have been used [37-39]. Magnetic fillers have also been used such as iron-oxide (Fe_xO_y) NPs (e.g., Fe3O4, γ-Fe2O3, etc.), cobalt ferrite ($CoFe_2O_4$), etc. [40, 41]. Strontium ferrite ($SrFe_{12}O_{19}$) is a hard magnetic material which possesses high coercivity due to its magnetocrystalline anisotropy [42]. It has not been explored to its full potential in fabrication of magnetic hydrogels.

In this work, attempts were made to prepare highly flexible, physically crosslinked and fully biodegradable PVA/CMC hydrogels with different magnetic nanoparticle content by moist heat treatment. This one-pot, simple, fast, inexpensive and facile preparation method allowed for easy fabrication of magnetic hydrogels. The effects of MG composition on physico-chemical properties of these hydrogels were examined to evaluate its usefulness as a biodegradable alternative for treatment of diabetic foot.

2. Experimental methodology

2.1 Materials

Polyvinyl alcohol (PVA: Mowiol® 28-99, molecular weight 145,000 Da) in form of flakes was purchased from Sigma Aldrich, Germany. Carboxymethyl cellulose (Na-CMC) powder of medium viscosity 800-1200 cps was supplied by Sinopharm Chemical Reagent Co. Ltd., Shanghai, China. Polyethylene glycol 3000 (PEG) flakes with molecular weight range between 2700-3300 and agar powder (3000-9000 MW) were obtained from Fluka, Switzerland. Anhydrous glycerine was obtained from Lachema, Brno, Czech Republic. Strontium ferrite ($SrFe_{17}O_{19}$) nanopowder <100 nm was used as the magnetic filler for the hydrogels, it was supplied by Sigma Aldrich, Germany. For ease of understanding the nanopowder will be denoted as MG. All solvents used during the experimental work were supplied by VWR Chemicals, France.

2.2 Preparation of PVA/CMC composite hydrogels

PVA/CMC hydrogels were fabricated using the moist heat treatment method. Solutions of base polymers, PVA (1wt%) and CMC (1wt%) solutions were prepared separately by dissolving in deionized water (DI) (40mL each) at temperature maintained at 80 °C for about 2h under continuous stirring. Then these two solutions were mixed together to prepare homogeneous mixture into which agar (1wt%), PEG (3wt%) and glycerine (3wt%) were added to the homogeneous mixture which acts as gelling agent, healing promoter and humectant, respectively [43]. To this mixture, SrFe nanoparticles (MG) previously sonicated in 20mL of DI water is added in varying concentrations such as 0.8wt%, 1.0wt% and 1.2wt%, respectively and the hydrogel samples are designated as PVA/CMC/MG 8, PVA/CMC/MG 10 and PVA/CMC/MG 12, respectively. Another hydrogel sample was prepared using the same composition but without the magnetic nanopowder and was used as control and designated as PVA/CMC (control). The detailed composition of each of the hydrogels is shown in Table 1. The samples were placed in an autoclave sterilizer which provides moist heat treatment (121 °C, 15 lbs/in^2) for 30 minutes. During this treatment the sterilization and crosslinking occurs in a single step as shown in Scheme 1. Subsequently, the solutions are poured into polystyrene casts and dried in hot air oven set at 25 °C for 48h approximately. As the liquid cools down the polymer chains form a 3-dimensional network and result in the formation of hydrogel which are termed as air-dried hydrogels (utility model

granted) [44]. Similarly, when the solutions poured into polystyrene casts are lyophilized, they are called freeze-dried hydrogels.

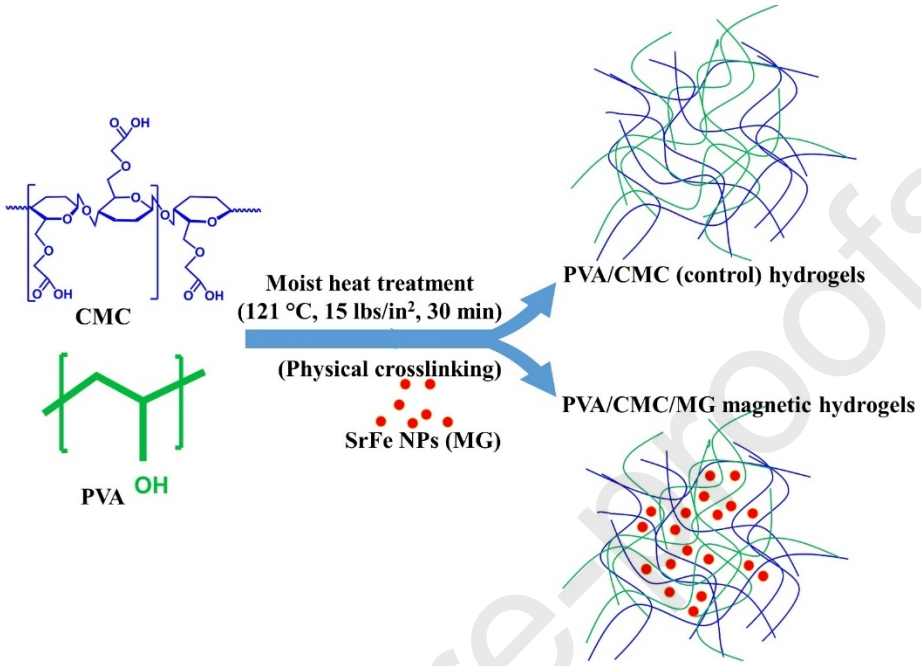

Scheme 1: Schematic representation of the preparation of PVA/CMC/MG hydrogels.

Table 1: Sample codes and composition of hydrogels used in this research work.

Sample code	PVA (g)	CMC (g)	PEG (g)	Agar (g)	Glycerin (g)	SrFe (g)	Water (mL)
PVA/CMC (control)	1	1	3	1	3	0	100
PVA/CMC/MG 8	1	1	3	1	3	0.8	100
PVA/CMC/MG 10	1	1	3	1	3	1.0	100
PVA/CMC/MG 12	1	1	3	1	3	1.2	100

2.3 Analytical instrumentation and characterization

To determine the physico-chemical properties of pure PVA, pure CMC, PVA/CMC (control) and PVA/CMC magnetic hydrogels, they were analysed by Nicolet 320 Fourier transformed infrared spectrophotometer (FTIR) (Thermo Scientific, USA) with a germanium ATR crystal. The attenuated total reflectance (ATR)-FTIR spectra were collected in the range 600-4000 cm^{-1} while room temperature, scan rate and resolution of 25 °C, 16 scans and 4 cm^{-1}, respectively were fixed for all measurements.

X-ray diffraction patterns of hydrogels and magnetic nanopowder were obtained using MiniFlex™ 600 X-ray diffractometer (Rigaku, Japan) with CoK_{β} as source (λ=1.79 Å). Operating voltage and current were maintained at 40 kV and 15 mA, respectively for all measurements. Diffractograms for all samples were captured from 2θ range 3°–90° with 10°/s as step time and 0.02° as a step size. All the data recorded using Co source are later converted to Cu source using software PowDLL converter to be able to compare the data with previous literature.

Control and magnetic PVA/CMC blend hydrogels solutions were lyophilized to get spumous samples. The cross-sectional surface was observed using Nova 450 nanoSEM scanning electron microscope (FEI, Thermo Fisher, USA) operated at high vacuum and 5kV accelerating voltage. The micrographs were obtained using secondary electron imaging mode at a magnification of 200x to 20 kx.

The tensile tests were conducted on a M350-5CT tensile testing machine (Testometric, UK) supplied with a 10 kgf load cell. Crosshead pull speed and gauge length of 10 mm/min and 20 mm, respectively were fixed for all measurements. Dumbbell shaped specimens were cut using a special

die (Type 3, ISO 37:2005). The Young's elastic modulus (MPa), ultimate tensile strength (N/mm), percentage elongation (%) and other mechanical properties were determined. Five samples of each composition were tested and averaged values with standard deviation are reported.

Thermal stability analysis was done using a TGA Q500 thermogravimetric analyzer (TA Instruments, USA). For each measurement sample weight, heating range, heating rate and N_2 flow rate were fixed at 9.0±1.0 mg, room temperature to 800 °C, 10 °C min^{-1} and 100 mL min^{-1}, respectively.

The PVA/CMC composite hydrogel samples (20.0±1.0 mg) sealed in aluminum pans were analyzed on a DSC1 STAR differential scanning calorimeter (Mettler Toledo, Switzerland). To estimate glass (phase) transition (T_g) and melting or fusion (T_m) temperatures, the samples were subjected to heating-cooling cycles at 10 °C min^{-1} ramping rates. Each specimen was heated from −70 °C to 160 °C during the first heating cycle followed by cooling down to −70 °C and then a final heating was done to 250 °C.

The DMA measurements were performed in linear viscoelastic region (LVR) at a heating rate of 5 °C/min and fixed frequency of 1 Hz on a DMA1 dynamic mechanical analyzer (Mettler Toledo, Switzerland). The hydrogel samples were cut with the help of a die in form of dumbells having dimensions of 15×1.9×~1.5mm. The temperature was ranged from. The variation in values of storage modulus (E′) and the loss factor (tan δ) were measured in the temperature range of -25 to 125 °C.

Swelling performance of the control and magnetic PVA/CMC hydrogels has been evaluated using the gravimetric technique. The air-dried hydrogels were cut into small pieces (25 mm diameter, 0.3-0.5 mm thickness), weighed and immersed in physiological saline (0.9% NaCl) solution (pH 7.40, 37 °C) for a total time period of 180 min in hot air oven maintained at 37 °C. After fixed intervals of time, the samples were retrieved from solution, the excess water on the surface of the swollen hydrogels was removed using wet absorbent papers and then the samples were weighed and again placed back in solution. The tests were conducted in triplicates and averaged values are reported along with standard deviation. The swelling ratio % was calculated as per Equation 1 [45].

$$\text{Swelling Ratio (\%)} = (W_s - W_d)/W_d \times 100 \quad (1)$$

where, W_s, W_d are weights of hydrogel sample in swollen and dry forms, respectively.

The surface free energy (SFE) and contact angle measurements for PVA/CMC (control) and magnetic hydrogels were carried out on goniometer (See System, Advex Instruments) at 21 °C. Two liquids viz. water and diiodomethane (DIM) were used for surface free energy calculations. Around 5 µl of liquid was dropped on the sample surface (10 × 10 mm^2) with the help of fixed-volume micropipette and drop shape was observed using a CCD camera. The contact angle was recorded after 1 min of stabilization time and average value from five samples were reported. The SFE for the hydrogel samples was determined by Owens, Wendt, Rabel and Kaelble (OWRK) method which is governed by Equation 2. The liquid surface tension (γ_L), polar fractions (γ_L) and disperse (γ_L^D) fractions were obtained from the literature [46].

$$\frac{1}{2}(1+cos\,\theta)\frac{\gamma_L}{\sqrt{\gamma_L^D}} = \sqrt{\gamma_S^P}\sqrt{\frac{\gamma_L^P}{\gamma_L^D}} + \sqrt{\gamma_S^D} \quad (2)$$

where, (γ_S) is the surface free energy of a solid.

The magnetic property measurements of PVA/CMC hydrogels were carried out on a vibrating sample magnetometer (VSM 7407, Lake Shore) at 21 °C in air atmosphere from -10kOe to 10 kOe range of applied magnetic field.

The viscoelastic property measurements of PVA/CMC swelled hydrogels samples (20 mm) were carried out using Anton Paar using the parallel plate geometry (20 mm). Dynamic frequency sweep analyses were done at 25 °C in oscillation mode with ω= 0.1 to 100 rad/s and 1% amplitude strain. The influence of magnetic filler loading on viscoelastic properties such as storage modulus (G′), loss modulus (G′′) and dynamic viscosity (η′) was calculated using Equation 3.

$$\eta^* = \left[\left(\frac{G'}{\omega}\right)^2 + \left(\frac{G''}{\omega}\right)^2\right]^{0.5} \quad (3)$$

3. Results and discussion

3.1 Physical observation of the PVA/CMC/MG composite hydrogels

Based on magnetic insoles, four samples of hydrogels i.e. PVA/CMC (control), PVA/CMC/MG 8, PVA/CMC/MG 10 and PVA/CMC/MG 12 were prepared. The images of the above mentioned hydrogels in air-dried and lyophilized forms are shown in Figure 1. The air-dried

hydrogels have a rubber like flexibility with a smooth texture and a well-defined shape. The PVA/CMC control air-dried hydrogels (Figure 1a) were translucent with off-white whereas the magnetic hydrogels were opaque and had a dark reddish-brown color (Figure 1(b-d)) which does not depend on the loading of the strontium nanoparticle concentration. Upon, lyophillization all the hydrogels attain a foam like appearance as shown in Figure 1(e-h) and become very light after losing all the inbound water.

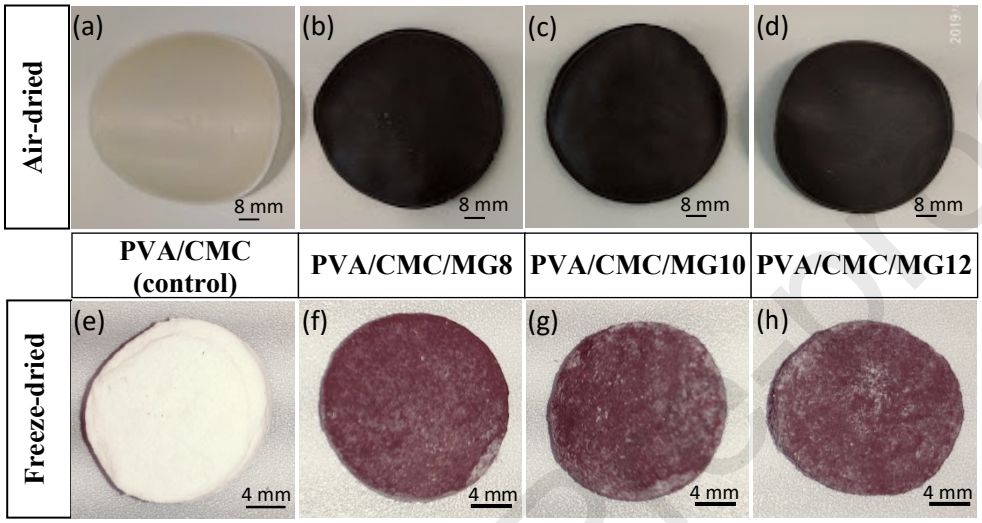

Figure 1: Optical images of air-dried (a-d) and freeze-dried (e-h) magnetic hydrogels: PVA/CMC (control) (a and e), PVA/CMC/MG 8 (b and f), PVA/CMC/MG 10 (c and g) and PVA/CMC/MG 12 (d and h), respectively.

3.2 Infrared Spectroscopy studies of PVA/CMC hydrogels

Infrared absorbance spectra of pristine PVA, pristine CMC, PVA/CMC (control) and PVA/CMC/MG magnetic hydrogels are illustrated in Figure 2. The IR spectra of PVA (Figure 2a(i)) shows a broad absorption band at 3310 cm^{-1} which ascribes to the O–H stretching of PVA hydroxyl groups [47]. The absorption band at 1677 cm^{-1} relates to the acetate group carbonyl (C=O) stretching. The peaks identified at 2940 and 2910 cm^{-1} correspond to the stretching vibration of C–H of backbone aliphatics [48]. Intense absorption bands on IR spectra were observed for C–O stretching and CH·OH combination frequencies at 1092 and 1325 cm^{-1}, respectively [47]. The IR spectra of CMC (Figure 2a(ii)) shows characteristic absorption band at 896, 1060, 1416, 1599, 2908, 3234 and 3446 cm^{-1} which attributes to the alcohol C–O stretching, β-1,4-glycosidic band, C=C, C=O carbonyl, C–H stretching and CMC sodium molecules

intermolecular hydrogen bonding, respectively [49]. The IR spectra of PVA/CMC hydrogel crosslinked by moist heat treatment renders unique features where new absorption bands emerge while few absorption bands disappeared as seen in Figure 2a(iii-iv). It can be observed for all PVA/CMC, intensity of hydrogen bonding peak is higher than CMC and is comparatively broader starting from 3017-3650 cm^{-1}. The probable reason for this could be the hydrogen bond formations between -COOH groups and non-substituted -OH groups of cellulose molecule which indicates that CMC interacts with PVA through hydrogen bonding [47].

3.3 X-ray diffraction analysis of PVA/CMC/MG hydrogels

The x-ray diffraction pattern of all hydrogels, constituent materials is shown in Figure 2b. The magnetic nanofiller used in this study was the strontium ferrite nanoparticles which was procured commercially. The major peaks appear at 30.4° (110), 32.4° (107), 34.1° (114) and 37.2° (203), respectively which matches with the library literature (JCPDS No. 80-1197) confirming the hexagonal M-type phase for SrFe (Figure 2b(i)). The PVA (Figure 2b(ii)) shows characteristic peak positioned at $2\theta=20.5°$ and a shoulder at around $2\theta=23.5°$ whereas, CMC (Figure 2b(iii)) shows a wide peak at $2\theta=20.5°$. Interestingly, the PVA/CMC hydrogels (Figure 2b(iv-vii)) exhibit sharp peak at 19.2° which indicates uniform blending of all the constituent polymers. A small peak at 23.5° can be seen which confirms the presence of PVA in the hydrogel blend. With the incorporation of magnetic nanoparticles, the peaks become intense and broad as the loading of strontium ferrite nanoparticles increases. This indicates towards the increase in crystallinity of the magnetic hydrogels.

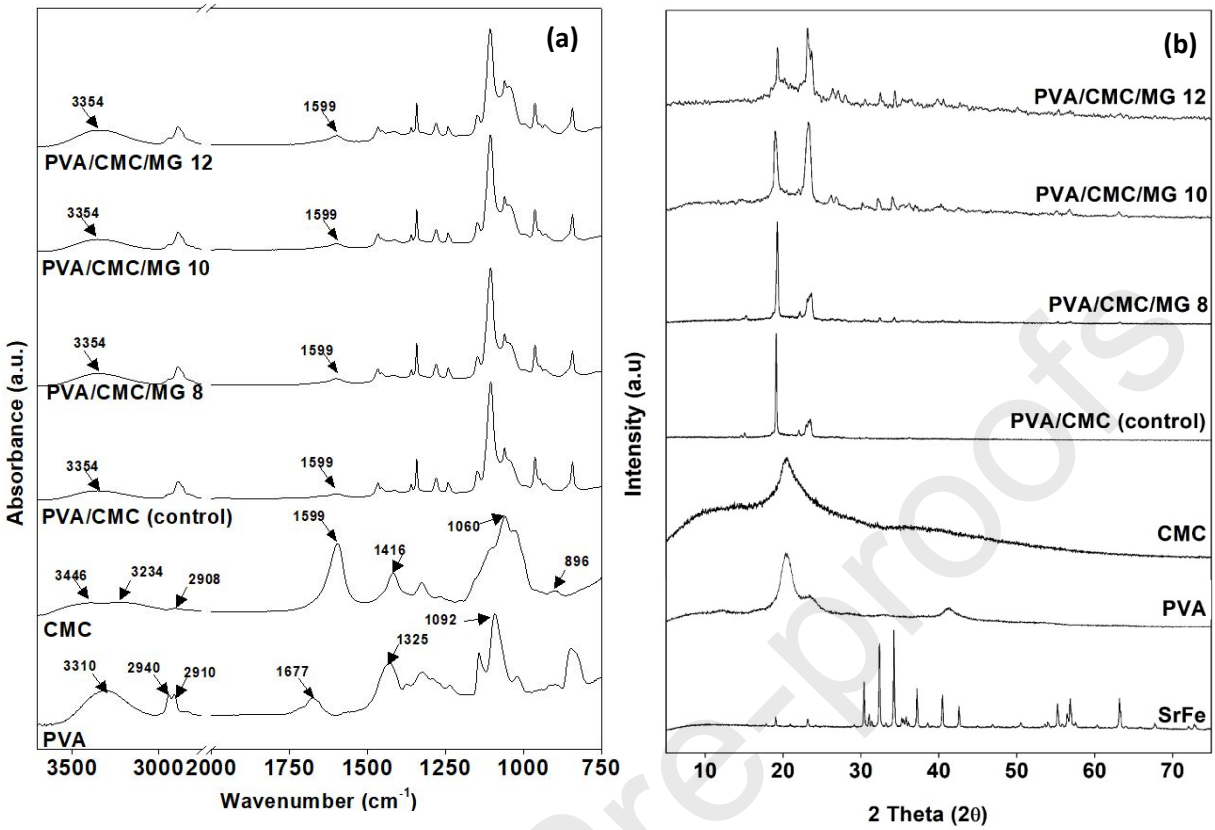

Figure 2: (a) FTIR spectra of different hydrogels (i) PVA; (ii) CMC; (iii) PVA/CMC (control); (iv) PVA/CMC/MG8; (v) PVA/CMC/MG10 and (vi) PVA/CMC/MG12 hydrogels; (b) X-ray diffraction patterns of (i) SrFe magnetic nanoparticles, (ii) PVA; (iii) CMC; (iv) PVA/CMC (control); (v) PVA/CMC/MG8; (vi) PVA/CMC/MG10 and (vii) PVA/CMC/MG12 hydrogels.

3.4 Morphological properties of PVA/CMC hydrogels

The cross-sectional morphology and surface topography of various lyophilized PVA/CMC hydrogels was examined using the scanning electron microscope (SEM). The cross-sectional view of PVA/CMC (control) hydrogel is shown in Fig. 3a, the pores are uniform throughout with pore walls smooth in texture (Figure 3a) and the surface view (Figure 3a′) shows the presence of the inter-polymeric networks forming the minute pores and the required stress transfer points. The surface of all PVA/CMC hydrogels shows globule like micron-sized particles which are homogenously distributed throughout the PVA/CMC matrix which is possibly PEG and glycerol. A clear change on the pore morphology in the cross-sectional micrographs (Figure 3b-3d) can be observed upon addition of magnetic nanoparticles. As the MG loading is increased the pores become irregular and the number of pores also reduce dramatically.

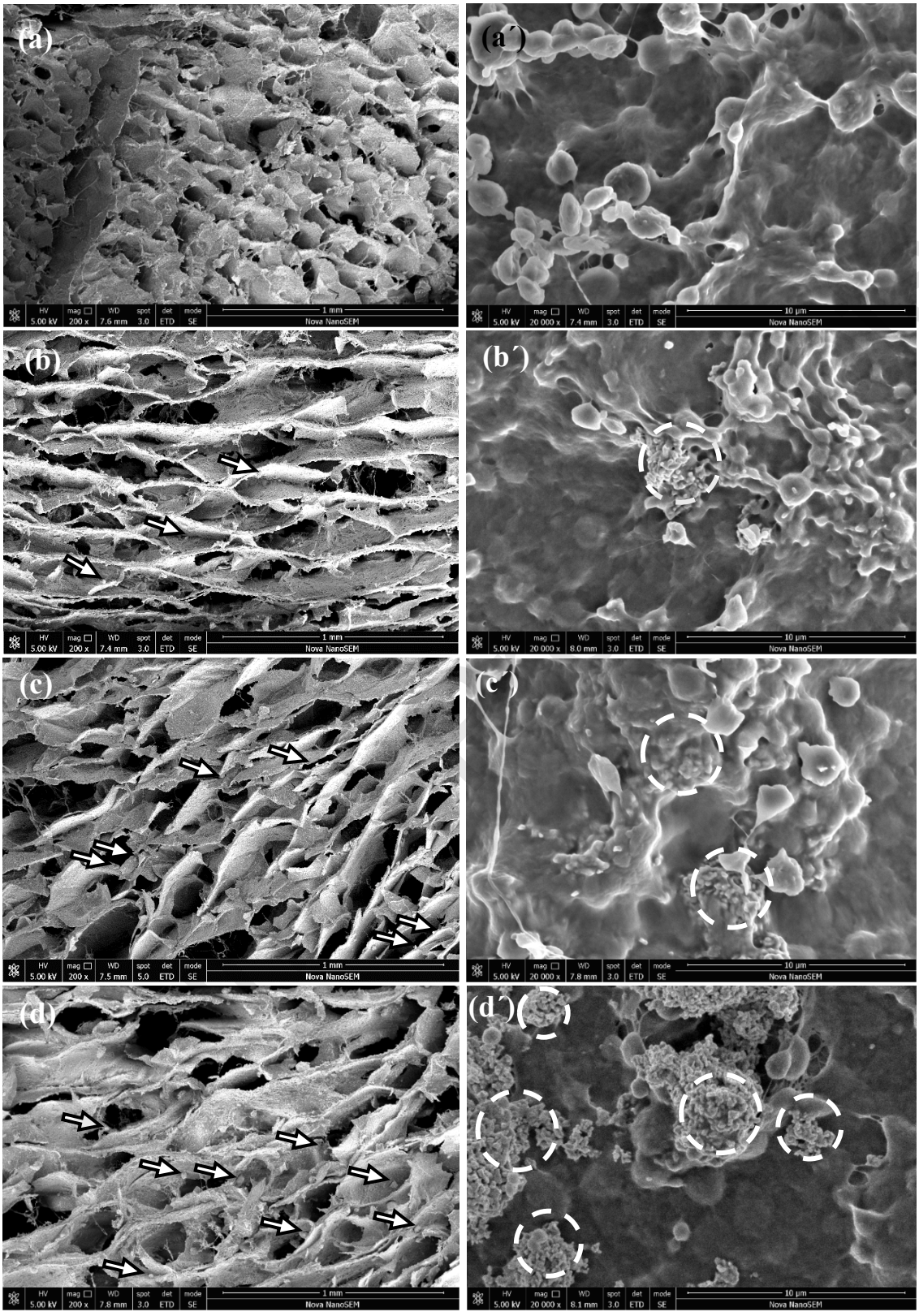

1

Figure 3: Scanning electron micrographs of cross-sectional view (a-d) and surface morphologies (a′-d′) of (a and a′) PVA/CMC (control); (b and b′) PVA/CMC/MG8; (c and c′) PVA/CMC/MG10 and (d and d′) PVA/CMC/MG12 hydrogels.

The pore walls become considerably rough due to the magnetic nanoparticles dispersed throughout the matrix shown in white arrows. The surface micrographs (Figure 3b′-3d′) of magnetic hydrogels captured at 20,000x shows that magnetic nanoparticles are uniformly dispersed in the PVA/CMC matrix. However, as the magnetic nanoparticle loading is increased the particle agglomeration is observed as shown in white dashed circles.

3.5 Mechanical testing of PVA/CMC/MG composite hydrogels

To evaluate the fabricated magnetic hydrogels for their utilization as shoe insoles for diabetics, mechanical analysis becomes very crucial. The materials should have desired strength and flexibility for long-term use. Figure 4 indicates the stress vs. strain curves for the PVA/CMC magnetic hydrogels with varying loading of magnetic nanofiller loadings. Here, it can be observed that incorporation of 10 wt% nanofiller within the PVA/CMC matrix increases the tensile strength and elongation. However, upon further increase the mechanical properties deteriorate gradually due to the formation of MG agglomerates throughout the matrix as can be observed from SEM micrographs.

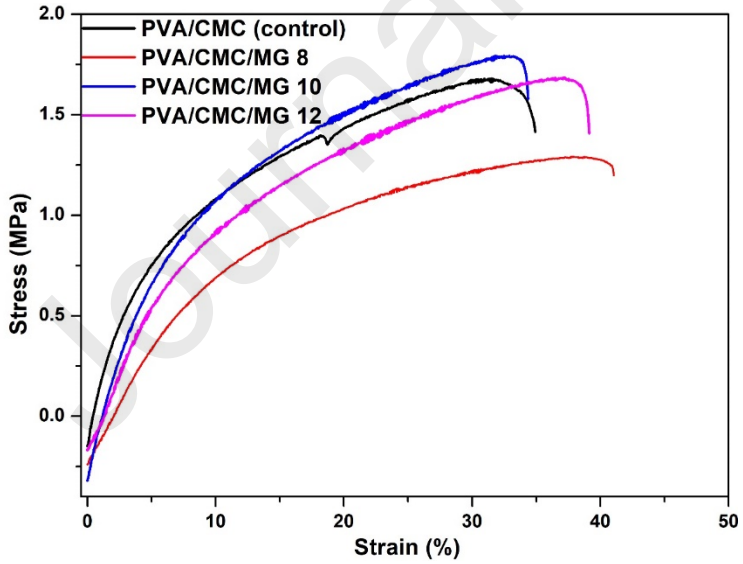

Figure 4: Stress vs. strain curves for various PVA/CMC hydrogels with different concentration of magnetic nanofiller loadings.

At 10wt% of optimum loading there is better interaction between the matrix and reinforcement which generates surface energy thus improving the mechanical properties. The values of tensile strength and elongation matches closely with the values of faux leather which is a commonly used material in shoe insoles [50]. The elastic modulus, ultimate tensile strength and percentage elongation of the PVA/CMC hydrogels are tabulated in Table 2.

Table 2: Summary of mechanical properties of the PVA/CMC hydrogel samples.

Hydrogels	Young's Modulus, E (MPa)	Ultimate Tensile Strength, σ (N/mm^2)	Elongation at Break, ε (%)	Stress at Break (MPa)
PVA/CMC (Control)	17.2±0.9	1.6±0.1	32.0±2.5	1.5±0.1
PVA/CMC/MG 8	8.5±3.6	1.3±0.1	42.5±1.0	1.3±0.1
PVA/CMC/MG 10	13.3±3.3	1.9±0.4	45.0±4.0	1.6±0.1
PVA/CMC/MG 12	11.8±1.7	1.8±0.1	49.0±1.0	1.7±0.1

3.6 Thermogravimetric analysis of prepared PVA/CMC hydrogels

Thermal stability plays a key role in determining the processing ability of any material and ultimately its applications. The thermal degradation profiles of magnetic nanoparticle filled PVA/CMC hydrogels were recorded using thermogravimetric analyzer by heating the hydrogel samples from room temperature to 800 °C under inert atmosphere and are shown as Figure 5a. In the derivative curves shown in Figure 5b, all PVA/CMC hydrogels feature a broad peak starting from 60 °C until 150 °C which indicates loss of bound water within the hydrogel. A prominent peak around 235-250 °C is observed for all PVA/CMC hydrogels which attributes to the polysaccharide decomposition where COO- group of CMC undergoes decarboxylation resulting into the formation of CO, CO_2 and CH_4 [45]. A small hump is also observed from 260-330 °C which relates to the degradation of PVA chains. Another peak is observed at ~400 °C which can be attributed to the degradation of polymers such as PVA and PEG [51]. A new peak at around 290 °C is observed for the magnetic hydrogels which ascribes to formation of hydroxides [52]. Another peak appears around 400 °C which is associated with the decomposition of nitrates and hydroxides. This peak overlays onto the polymer matrix degradation peak which is the reason for the increased intensity.

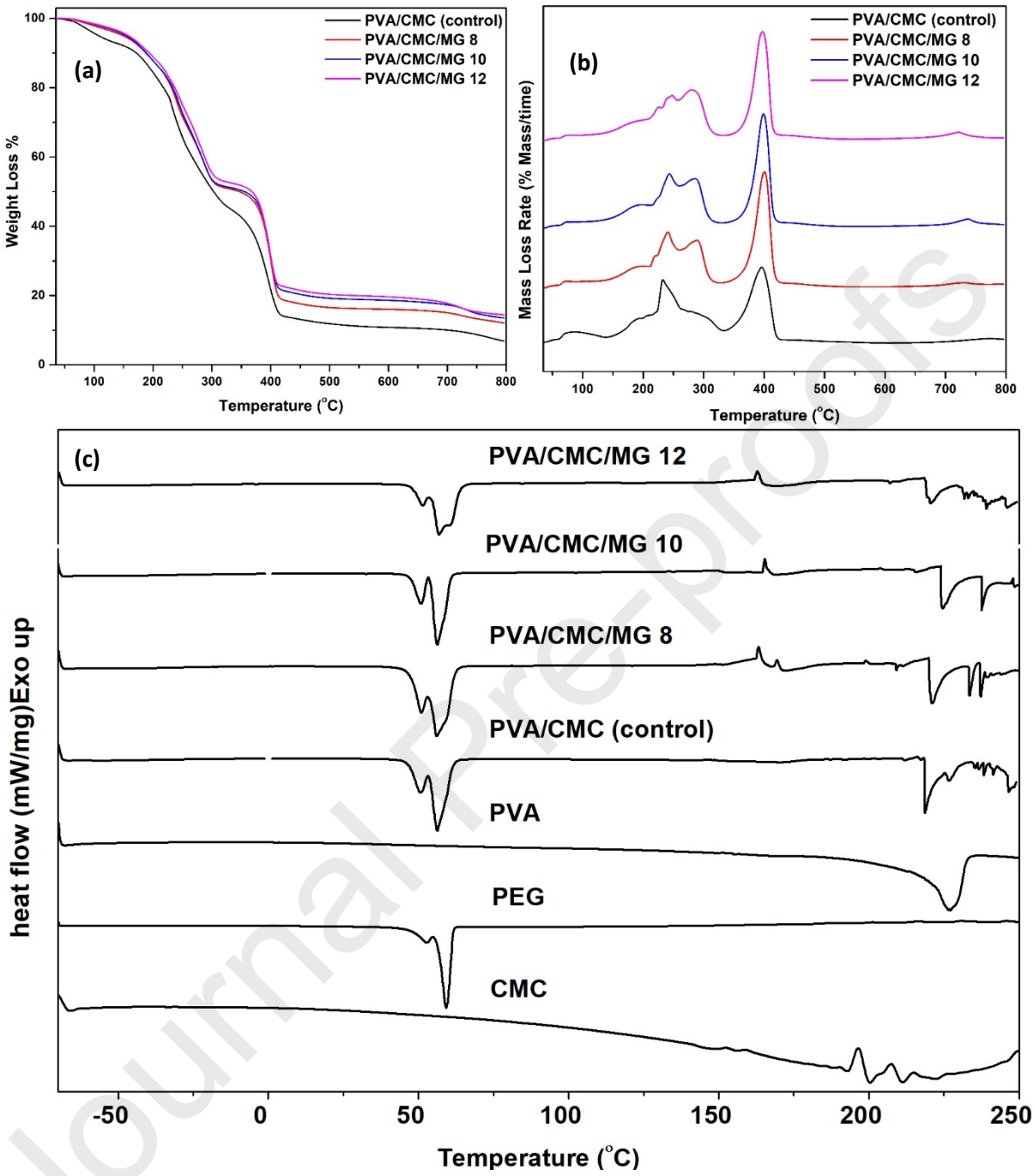

Figure 5: (a) TGA (b) DTG and (c) DSC curves for PVA/CMC (control) and PVA/CMC/MG magnetic hydrogels.

3.7 Dynamic scanning calorimetry (DSC) studies of PVA/CMC/MG hydrogels

Figure 5c shows the second heating DSC scans for the PVA/CMC (control) and magnetic hydrogels. It is noteworthy to mention that no glass transition points were observed on the DSC

thermograms. However, two endothermic peaks around 50 °C and around 220 °C were observed which are the melting peaks of PEG and PVA, respectively [53, 54]. The PEG melting temperatures were not much affected upon incorporation of magnetic nanoparticles but melting temperature for PVA got influenced. The Tm for PVA/CMC (control) and magnetic hydrogels (8, 10 and 12wt%) were found to be 219.0, 221.0, 225.0 and 221.0 °C, respectively. It can be seen that magnetic nanofillers produce heterogenous nucleation effect resulting in more stable magnetic hydrogels which can also be evidenced from mechanical analysis [55]. The increase in melting point did not lead to increase in melting enthalpies for magnetic hydrogels which were found to be 12.6 J/g (8wt%), 13.3 J/g (10wt%) and 11.2 J/g (12wt%) as against 14.7 J/g for PVA/CMC (control) hydrogels.

3.8 Thermomechanical property analysis of PVA/CMC hydrogels

For all hydrogel samples, the DMA findings (variation of storage modulus (E′) and loss factor (tan δ) versus temperature) for control and magnetic hydrogels show a similar trend as the temperature was increased as seen in Figure 6. From Figure 6a, it was found that below $T_{g,PVA}$ (60.8 °C), storage modulus values were having a high magnitude which dropped gradually as the temperature increased. In the temperature range of -25 °C to room temperature, hydrogels were in glassy state with rigidity which can be seen from high E′values. At 25 °C, E′values of 16.1, 31.9, 60.7 and 29.1 MPa were observed for control, 8wt%, 10wt% and 12wt% loaded hydrogels, respectively which showed that 10wt% loading was the optimum loading. Such higher storage modulus values as compared to control hydrogel could possibly be due to the homogeneous distribution of magnetic nanoparticles in the PVA/CMC matrix allowing effective stress transfer. Similar results were also observed from mechanical tensile tests. As the temperature increased the hydrogels underwent a glassy-rubbery phase transition which can be characterized by sudden fall in storage modulus values (Figure 6a) and appears as a maxima in tan δ curves (Figure 6b). The PVA glass transition temperature was observed at 60.8 °C which matches closely with the 61 °C as reported by Lorenzo et al. [56]. However, a reduction in T_g (observed from tan δ curves) was observed upon incorporation of magnetic nanoparticles viz. 60.8, 51.1, 54.1 and 51.8 °C for 8, 10 and 12wt% loading, respectively. The spherical-shaped magnetic nanoparticles impart a plasticizing effect thus causing reductions in T_g which can be corroborated from elongation results from mechanical analysis [57].

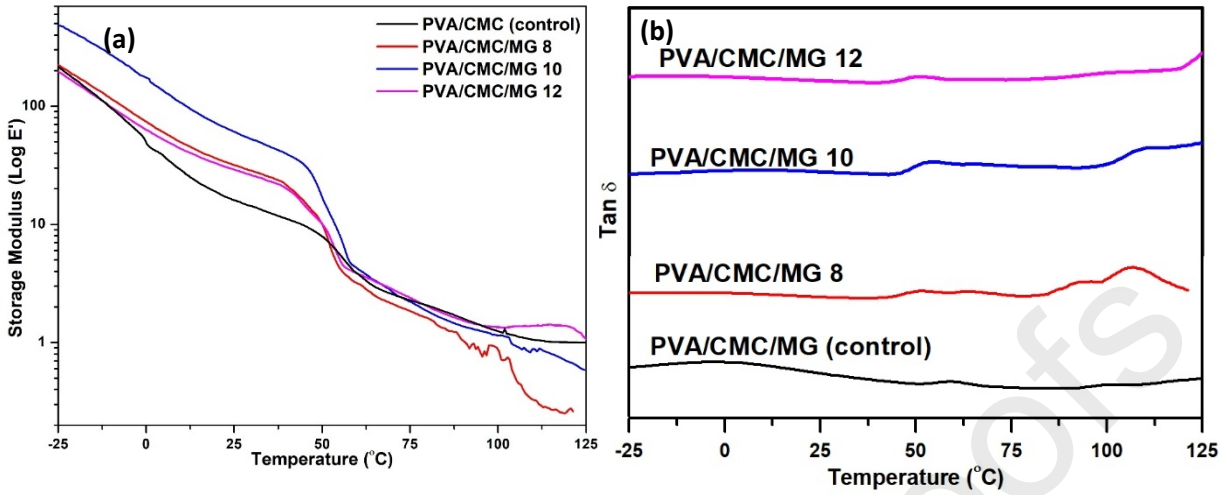

Figure 6: Variation in thermomechanical properties, (a) storage modulus (E′) and (b) loss factor (tan δ) as a function of temperature with increasing MG loading (wt%).

3.9 Swelling behavior of PVA/CMC/MG magnetic hydrogels

Figure 7a shows the swelling character of the magnetic hydrogels. All the samples showed growth in swelling ratio at first followed by equilibrium at approximately 90 minutes. The pure PVA/CMC (control) discs showed the maximum equilibrium swelling percentage of 325% as compared to the magnetic hydrogels having 290%, 260% and 250% for 10wt%, 12wt% and 8wt%, respectively. It is noteworthy to mention that the presence of magnetic nanoparticles inside the hydrogels results in cross-linked structures that reduce the pores thus the available volume for water molecules to penetrate inside ultimately lowering the swelling behavior and water retention capacity. Furthermore, the strontium ferrite magnetic nanoparticles lack the ability to absorb water.[58, 59] Among all the magnetic hydrogels, 10wt% loading exhibited the highest swelling ratio possibly due to the homogeneous dispersion of magnetic nanoparticles without agglomeration whereas 8wt% and 12 wt% loading showed lower swelling behavior possibly due to poor mechanical properties as can be seen in Figure which affects the integrity upon water absorption [60].

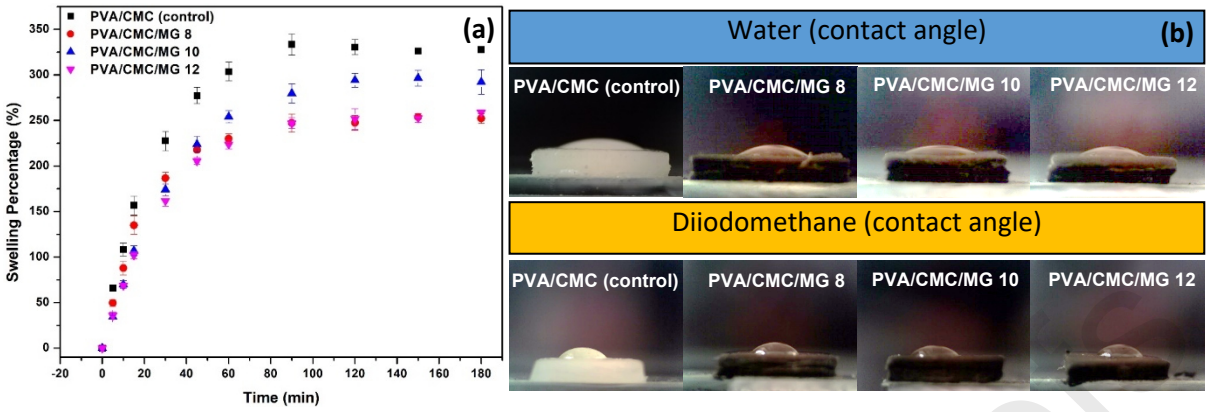

Figure 7: (a) Variation in swelling behavior as a function of time and (b) images of contact angles with water and diiodomethane for PVA/CMC (control) and PVA/CMC/MG magnetic hydrogels.

3.10 Contact angle and surface free energy (SFE) calculations

Effect of incorporation of magnetic nanoparticles on wetting characteristics of hydrogels such as contact angle and SFE were measured using polar (water) and non-polar (diiodomethane) solvents and representative images are shown in Figure 7b. The contact angles shown in Table 3 for all hydrogels are less than 90° which means that all hydrogels are hydrophilic in nature. This will aid in sweat absorption during long hours of wearing the shoe insoles. This can avoid the growth of harmful microbes and indirectly check the odor, which is an important feature missing in conventional shoe insoles available in market.

Table 3: contact angle and surface free energy (SFE) values for control and magnetic hydrogels. (DIM: diiodomethane)

Hydrogels	**Contact angle**		**Surface free energy (γ_S), mN/m**	**Polar (γ_S)**	**disperse (γ_S^D)**
	water	**DIM**			
PVA/CMC (control)	25.2	45.4	69.8	36.8	33.0
PVA/CMC/MG 8	30.9	44.4	67.3	37.3	30.0
PVA/CMC/MG 10	27.9	50.4	67.5	34.03	33.5
PVA/CMC/MG 12	29.9	41.5	68.4	38.8	29.6

The magnetic hydrogels get less hydrophilic which can be seen by greater contact angles 30.9±1.0, 27.9±0.6 and 29.9±2.3 for 8,10 and 12wt% loading as against 25.2±1.1 for PVA/CMC (control)

hydrogels. The plausible reason for higher contact angles is the addition of magnetic nanoparticles which are known to be hydrophobic in nature [61]. Surface free energies for all magnetic hydrogels (8, 10 and 12wt%) are 67.3, 67.5 and 68.4 mN/m, respectively which is lower than that of control i.e. 69.8 mN/m, this suggests that the presence of magnetic nanoparticles impart hydrophobicity to the magnetic hydrogels.

3.11 Magnetic properties of CMC/PVA/MG hydrogels

In order to analyze the magnetic properties of the fabricated hydrogels, hysteresis loops were recorded using vibrating sample magnetometer (VSM) and are shown in Figure 8a and tabulated in Table 4. It can be seen that saturation magnetization (M_s), remanent magnetization (M_r), coercivity (H_c) as well as maximum energy product (BHmax) of stronitium ferrite nanoparticles are greater than prepared hydrogels. The plausible reason for the reduced values could be the isolation effects caused by polymers, where polymers get in between ferrite grains which creates demagnetizing field making the hydrogels weaker in magnetic character [62]. 10wt% loading of magnetic nanoparticles in the hydrogels provided superior magnetic performance due to uniform dispersion throughout the polymer matrix which can be seen as high values of M_s, M_r, H_c and BH_{max}.

Table 4: Magnetic properties of strontium ferrite nanoparticles and fabricated PVA/CMC/MG magnetic hydrogels.

Properties	**SrFe**	**CMC/PVA/MG 8**	**CMC/PVA/MG 10**	**CMC/PVA/MG 12**
BH_{max}, Goe	8.9×10^5	345.2 ± 47.4	512.9 ± 60.3	442.7 ± 23.7
B_r, G	2096.6	37.6 ± 3.0	45.5 ± 2.7	42.7 ± 1.4
Coercivity, H_c, Oe	4592.1	4630.9 ± 2.2	4658 ± 20.3	4633.8 ± 19.6
Saturation magnetization (M_s), emu/g	51.5	3.6 ± 0.2	4.3 ± 0.2	4.0 ± 0.2
Remanent magnetization (M_r), emu/g	32.2	2.2 ± 0.1	2.7 ± 0.1	2.5 ± 0.1

It is noteworthy to mention that PVA/CMC/MG magnetic hydrogels were able to achieve ~50G of magnetic power as against 400-450G provided by shoe inserts available in market [13]. However, sweat absorption, biocompatible, anti-odor features allow the PVA/CMC/MG based

magnetic insoles to be worn over longer periods of time for the desired effect. Intrestingly, increasing the loading to 12wt% lead to agglomeration and lead to settling down of magnetic particles which reduced the ferromagnetism of the composite [63]. The lower value of magnetic moment in PVA/CMC/MG 8 could be attributed to the higher content of polymers which do not contribute to magnetic character thus leading to decrease in magnetization value.

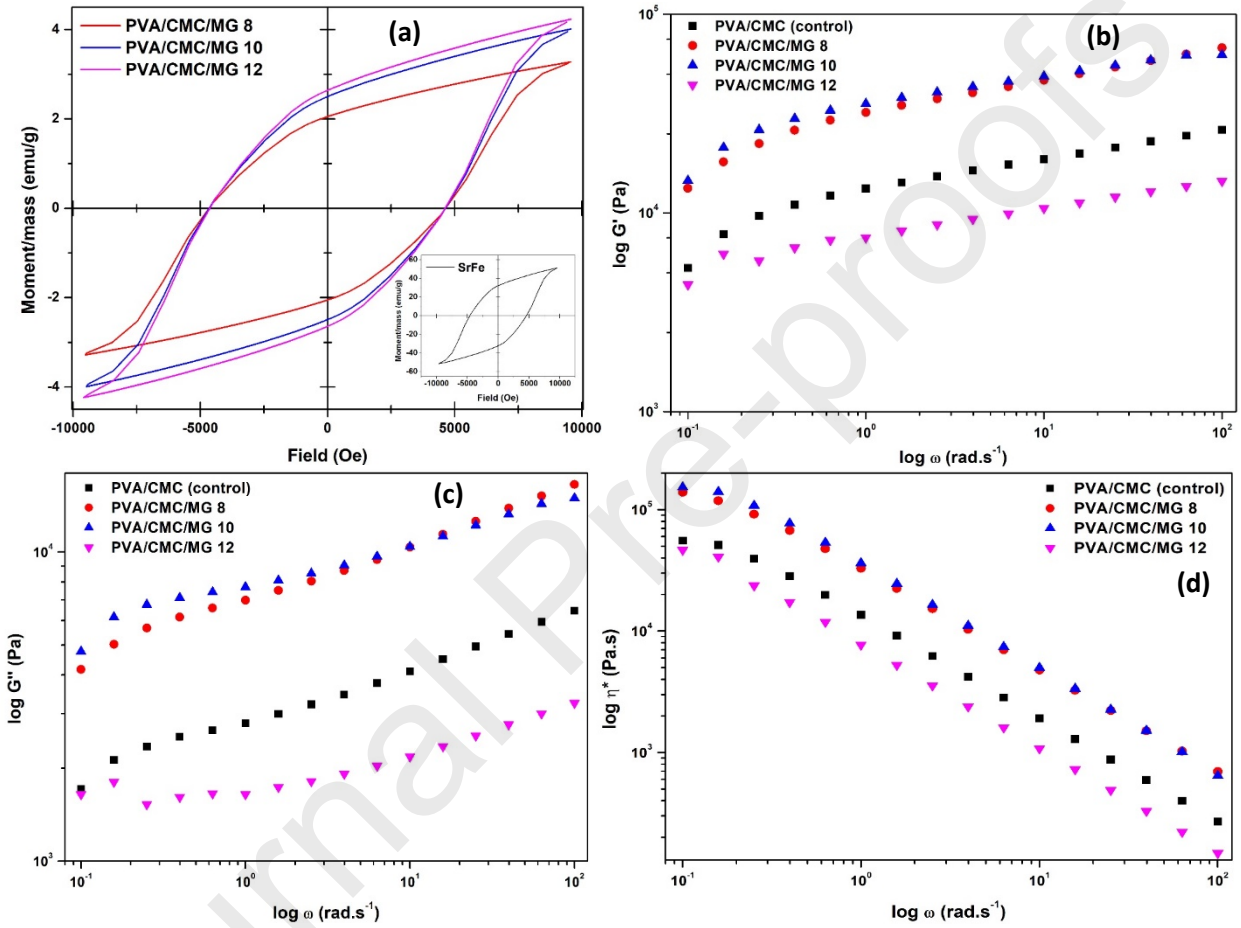

Figure 8: (a) Magnetization curves for PVA/CMC/MG magnetic hydrogels, inset: Magnetization curves of strontium ferrite nanoparticles, (b) Effect of angular frequency (α) at 1% strain on (a) storage modulus (G′), (b) loss modulus (G′′) and (c) complex viscosity (η*) for PVA/CMC/MG magnetic hydrogels.

3.12 Viscoelastic behavior of PVA/CMC/MG hydrogels

Using the rheological characterization especially the storage modulus (G′) and loss modulus (G′′) the elasticity and viscosity of the material can be determined. As can be seen from the Figures 8a and 8b, the G′ of all hydrogel samples is higher than their G′′ across the complete range of

angular frequency (ω=0.1-100 rad.s^{-1}), this elastic behavior is typical of hydrogels [64]. Due to physical interactions in the system, the G′ of magnetic hydrogels was greater than PVA/CMC (control) hydrogels indicating improved crosslinking. At ω = 10 rad.s^{-1}, the G′ values of control, 8wt%, 10wt% and 12wt% hydrogels were 15.9, 46.7, 48.8 and 10.6 kPa, respectively. The CMC/PVA/MG 10 demonstrated the highest values which could be corroborated from the results of mechanical analysis suggesting towards uniform dispersion of magnetic nanoparticles which lead to better shear transfer. Further increase in filler concentration to 12wt% leads to agglomeration which decreased crosslinking between CMC and PVA which can be seen in the poor storage modulus values [65]. Viscosity was also found to be increased upon addition of magnetic nanoparticles over the ω of 0.1–100 rad/s as depicted in Fig. 4b which indicates formation of a more rigid network [66].

4. Conclusions

This work provides a facile one-step process to synthesize novel PVA/CMC based magnetic hydrogels having different amounts of strontium ferrite nanoparticles for diabetic shoe insoles. Specifically, this technique and composition has arisen as a very effective tool for the production of flexible and biodegradable magnetic hydrogels. PVA/CMC/MG hydrogels were subjected to systemic and detailed structural, morphological, mechanical, thermal, magnetic, surface and visco-elastic characterization by FTIR, XRD, SEM, UTM, TGA, DSC, DMA, VSM, contact angle and rheometer to obtain fundamental information. Infrared analysis indicates that CMC interacts with PVA through hydrogen bonding. The presence of magnetic nanoparticles dramatically reduced the number of pores as well as pore size and also made the pores more irregular. Surface energy and contact angle measurements reveal that magnetic hydrogels are hydrophilic. hence can be effective sweat absorbers, thus keeping a check on growth of harmful microbes. The magnetic hydrogels showed more thermal stability as compared to control without magnetic loading. Swelling studies was performed as a function of time and a decrease in water absorption was observed by introduction of magnetic nanoparticles which creates additional physical cross-link. It can be concluded from the results that the incorporation of strontium ferrite nanoparticles to PVA/CMC has rendered filled hydrogels mechanically robust as can be seen from increased percentage elongation and tensile strength. Frequency sweep rheological measurements confirm the enhanced viscoelastic properties of magnetic hydrogels with increasing nanopowder loading.

The future works target is to improve magnetic properties of these hydrogels by using anisotropic nanoparticles. The simple, fast and inexpensive preparation method, absence of toxic chemicals, ability to absorb sweat and biodegradability suggest the PVA/CMC based magnetic hydrogels as a desirable alternative for non-degradable plastic based magnetic shoe insoles for prevention of diabetic foot.

Conflict of interest

None.

Acknowledgements

This research work is supported by Ministry of Education, Youth and Sports (MEYS) of the Czech Republic- Program NPU I (LO1504) and International Mobility of TBU researchers – CZ.02.2.69/0.0/0.0/16_027/0008464. We would also like to acknowledge Centre of Polymer Systems (CPS) situated at Tomas Bata University in Zlin, Czech Republic for permitting to use the available research facilities to conduct this research work.

Data Availability

The data that support the findings of this study are available from the corresponding author [N. Saha] upon reasonable request.

References

[1] B. Kronsteiner, P. Chaichana, M. Sumonwiriya, K. Jenjaroen, F.R. Chowdhury, S. Chumseng, P. Teparrukkul, D. Limmathurotsakul, N.P. Day, P. Klenerman, Diabetes alters immune response patterns to acute melioidosis in humans, Eur. J. Immunol., 49 (2019) 1092-1106.

[2] E.L. Feldman, B.C. Callaghan, R. Pop-Busui, D.W. Zochodne, D.E. Wright, D.L. Bennett, V. Bril, J.W. Russell, V. Viswanathan, Diabetic neuropathy, Nature Reviews Disease Primers, 5 (2019) 41.

[3] K.R. Ylitalo, M. Sowers, S. Heeringa, Peripheral vascular disease and peripheral neuropathy in individuals with cardiometabolic clustering and obesity: National Health and Nutrition Examination Survey 2001–2004, Diabetes care, 34 (2011) 1642-1647.

[4] A.K. Hamidi, S.M. Arzaghi, M. Qorbani, F. Khatami, M. Ebrahimi, F. Bandarian, S. Enayati, M.M. Amoli, MIF 173 G> C variation was associated with depressive disorder in type 2 diabetes in an Iranian population, Psychoneuroendocrinology, 104 (2019) 243-248.

[5] T. Thiruvoipati, C.E. Kielhorn, E.J. Armstrong, Peripheral artery disease in patients with diabetes: Epidemiology, mechanisms, and outcomes, World journal of diabetes, 6 (2015) 961.

[6] M.M.T.M. Win, K. Fukai, H.H. Nyunt, Y. Hyodo, K.Z. Linn, Prevalence of peripheral neuropathy and its impact on activities of daily living in people with type 2 diabetes mellitus, Nurs. Health Sci., 21 (2019) 445-453.

[7] Z. Sayiner, F. Can, E. Akarsu, Patients' clinical charecteristics and predictors for diabetic foot amputation, Primary care diabetes, 13 (2019) 247-251.

[8] I. Kruse, S. Edelman, Evaluation and treatment of diabetic foot ulcers, Clinical diabetes, 24 (2006) 91-93.

[9] S. Borys, A. Ludwig-Slomczynska, M. Seweryn, J. Hohendorff, T. Koblik, J. Machlowska, B. Kiec-Wilk, P. Wolkow, M.T. Malecki, Negative pressure wound therapy in the treatment of diabetic foot ulcers may be mediated through differential gene expression, Acta diabetologica, 56 (2019) 115-120.

[10] U. Dhamodharan, A. Karan, D. Sireesh, A. Vaishnavi, A. Somasundar, K. Rajesh, K.M. Ramkumar, Tissue-specific role of Nrf2 in the treatment of diabetic foot ulcers during hyperbaric oxygen therapy, Free Radical Biology and Medicine, 138 (2019) 53-62.

[11] W. Tettelbach, S. Cazzell, F. Sigal, J.M. Caporusso, P.S. Agnew, J. Hanft, C. Dove, A multicentre prospective randomised controlled comparative parallel study of dehydrated human umbilical cord (EpiCord) allograft for the treatment of diabetic foot ulcers, International wound journal, 16 (2019) 122-130.

[12] J. Paton, G. Bruce, R. Jones, E. Stenhouse, Effectiveness of insoles used for the prevention of ulceration in the neuropathic diabetic foot: a systematic review, J. Diabetes Complicat., 25 (2011) 52-62.

[13] M.I. Weintraub, G.I. Wolfe, R.A. Barohn, S.P. Cole, G.J. Parry, G. Hayat, J.A. Cohen, J.C. Page, M.B. Bromberg, S.L. Schwartz, Static magnetic field therapy for symptomatic diabetic neuropathy: a randomized, double-blind, placebo-controlled trial, Archives of physical medicine and rehabilitation, 84 (2003) 736-746.

[14] C.Y. Webb, S.S. Lo, J.H. Evans, Prevention of diabetic foot using low frequency magnetotherapy, The Diabetic Foot, 6 (2003) 138-145.

[15] N. Giordano, P. Papakostas, E. Battisti, A. Albanese, M. Rigato, A. Montella, R. Nuti, Magnetotherapy—a brief excursion through the centuries, The Environmentalist, 29 (2009) 157-160.

[16] M.M. Bhatti, M.M. Rashidi, Study of heat and mass transfer with Joule heating on magnetohydrodynamic (MHD) peristaltic blood flow under the influence of Hall effect, Propulsion and Power Research, 6 (2017) 177-185.

[17] K.S. Mekheimer, M.A. El Kot, Influence of magnetic field and Hall currents on blood flow through a stenotic artery, Applied Mathematics and Mechanics, 29 (2008) 1093.

[18] M.H. Winemiller, R.G. Billow, E.R. Laskowski, W.S. Harmsen, Effect of magnetic vs sham-magnetic insoles on nonspecific foot pain in the workplace: a randomized, double-blind, placebo-controlled trial, Mayo Clin. Proc., 80 (2005) 1138-1145.

[19] P. Tinley, A. Meneghello, M. Hey, Randomised double-blind crossed-over control trial to determine the therapeutic effect of Nikken® magnetic insoles (Magsteps®) in the treatment of plantar fasciitis, Journal of foot and ankle research, 8 (2015) P15.

[20] K.B. Landorf, A.-M. Keenan, R.D. Herbert, Effectiveness of different types of foot orthoses for the treatment of plantar fasciitis, Journal of the American Podiatric Medical Association, 94 (2004) 542-549.

[21] M. Iqbal, N. Iqbal, I.A. Bhatti, N. Ahmad, M. Zahid, Response surface methodology application in optimization of cadmium adsorption by shoe waste: a good option of waste mitigation by waste, Ecological engineering, 88 (2016) 265-275.

[22] X. Yang, J. Liu, Y. Wu, J. Liu, F. Cheng, X. Jiao, G. Lai, Fabrication of UV-curable solvent-free epoxy modified silicone resin coating with high transparency and low volume shrinkage, Progress in Organic Coatings, 129 (2019) 96-100.

[23] B. Lu, H. Yuk, S. Lin, N. Jian, K. Qu, J. Xu, X. Zhao, Pure PEDOT: PSS hydrogels, Nature communications, 10 (2019) 1043.

[24] L. Jaiswal, S. Shankar, J.-W. Rhim, Carrageenan-based functional hydrogel film reinforced with sulfur nanoparticles and grapefruit seed extract for wound healing application, Carbohydrate polymers, (2019) 115191.

[25] X. Wu, L. Black, G. Santacana-Laffitte, C.W. Patrick Jr, Preparation and assessment of glutaraldehyde-crosslinked collagen–chitosan hydrogels for adipose tissue engineering, Journal of biomedical materials research Part A, 81 (2007) 59-65.

[26] C. Xiao, Current advances of chemical and physical starch-based hydrogels, Starch, 65 (2013) 82-88.

[27] A. Dodero, L. Pianella, S. Vicini, M. Alloisio, M. Ottonelli, M. Castellano, Alginate-based hydrogels prepared via ionic gelation: an experimental design approach to predict the crosslinking degree, Eur. Polym. J., 118 (2019) 586-594.

[28] Q. Yang, Y. Yan, X. Yang, G. Liao, D. Wang, H. Xia, Enzyme immobilization in cage-like 3D-network PVA-H and GO modified PVA-H (GO@ PVA-H) with stable conformation and high activity, Chemical Engineering Journal, 372 (2019) 946-955.

[29] E. Caló, J.M. de Barros, M. Fernández-Gutiérrez, J. San Román, L. Ballamy, V.V. Khutoryanskiy, Antimicrobial hydrogels based on autoclaved poly (vinyl alcohol) and poly (methyl vinyl ether-alt-maleic anhydride) mixtures for wound care applications, RSC Advances, 6 (2016) 55211-55219.

[30] A. Mondino, M. Gonzalez, G. Romero, E. Smolko, Physical properties of gamma irradiated poly (vinyl alcohol) hydrogel preparations, Radiation Physics and chemistry, 55 (1999) 723-726.

[31] N. Roy, N. Saha, T. Kitano, P. Saha, Novel hydrogels of PVP–CMC and their swelling effect on viscoelastic properties, Journal of Applied Polymer Science, 117 (2010) 1703-1710.

[32] A. Gregorová, N. Saha, T. Kitano, P. Sáha, Hydrothermal effect and mechanical stress properties of carboxymethylcellulose based hydrogel food packaging, Carbohydrate polymers, 117 (2015) 559-568.

[33] M. Buraidah, A. Arof, Characterization of chitosan/PVA blended electrolyte doped with NH4I, Journal of Non-Crystalline Solids, 357 (2011) 3261-3266.

[34] M. Saadiah, D. Zhang, Y. Nagao, S. Muzakir, A. Samsudin, Reducing crystallinity on thin film based CMC/PVA hybrid polymer for application as a host in polymer electrolytes, Journal of Non-Crystalline Solids, 511 (2019) 201-211.

[35] M. Wang, L. Xu, H. Hu, M. Zhai, J. Peng, Y. Nho, J. Li, G. Wei, Radiation synthesis of PVP/CMC hydrogels as wound dressing, Nuclear Instruments and Methods in Physics Research Section B: Beam Interactions with Materials and Atoms, 265 (2007) 385-389.

[36] A. El Sayed, S. El-Gamal, Synthesis and investigation of the electrical and dielectric properties of Co3O4/(CMC+ PVA) nanocomposite films, J. Polym. Res., 22 (2015) 97.
[37] H. Dai, Y. Huang, H. Huang, Eco-friendly polyvinyl alcohol/carboxymethyl cellulose hydrogels reinforced with graphene oxide and bentonite for enhanced adsorption of methylene blue, Carbohydrate polymers, 185 (2018) 1-11.
[38] S. El-Gamal, A.M. El Sayed, E. Abdel-Hady, Effect of cobalt oxide nanoparticles on the nano-scale free volume and optical properties of biodegradable CMC/PVA films, Journal of Polymers and the Environment, 26 (2018) 2536-2545.
[39] A.M. El Sayed, S. El-Gamal, W.M. Morsi, G. Mohammed, Effect of PVA and copper oxide nanoparticles on the structural, optical, and electrical properties of carboxymethyl cellulose films, J. Mater. Sci., 50 (2015) 4717-4728.
[40] A. Brunsen, S. Utech, M. Maskos, W. Knoll, U. Jonas, Magnetic composite thin films of FexOy nanoparticles and photocrosslinked dextran hydrogels, Journal of Magnetism and Magnetic Materials, 324 (2012) 1488-1497.
[41] R. Messing, N. Frickel, L. Belkoura, R. Strey, H. Rahn, S. Odenbach, A.M. Schmidt, Cobalt ferrite nanoparticles as multifunctional cross-linkers in PAAm ferrohydrogels, Macromolecules, 44 (2011) 2990-2999.
[42] D.H. Chen, Y.Y. Chen, Synthesis of strontium ferrite nanoparticles by coprecipitation in the presence of polyacrylic acid, Mater. Res. Bull., 37 (2002) 801-810.
[43] N. Roy, N. Saha, T. Kitano, P. Saha, Development and characterization of novel medicated hydrogels for wound dressing, Soft Materials, 8 (2010) 130-148.
[44] R. Patwa, N. Saha, T. Sáha, P. Sáha, Obuvnická stélka s magneto-terapeutickými účinky, zejména pro diabetiky (Shoe insole with magneto-therapeutic effects, especially for diabetics), in: C.R. Úřad Průmyslového Vlastnictví (Ed.), Univerzita Tomáše Bati ve Zlíně, Zlín, CZ, Czech Republic, 2019, pp. 10.
[45] R. Shah, N. Saha, P. Saha, Influence of temperature, pH and simulated biological solutions on swelling and structural properties of biomineralized (CaCO 3) PVP–CMC hydrogel, Progress in biomaterials, 4 (2015) 123-136.
[46] R. Patwa, A. Kumar, V. Katiyar, Effect of silk nano-disc dispersion on mechanical, thermal, and barrier properties of poly (lactic acid) based bionanocomposites, Journal of Applied Polymer Science, (2018).

[47] M.F.A. Taleb, H.A. El-Mohdy, H.A. El-Rehim, Radiation preparation of PVA/CMC copolymers and their application in removal of dyes, Journal of hazardous materials, 168 (2009) 68-75.

[48] A.H. Pandit, N. Mazumdar, K. Imtiyaz, M.M.A. Rizvi, S. Ahmad, Periodate-Modified Gum Arabic Cross-linked PVA Hydrogels: A Promising Approach toward Photoprotection and Sustained Delivery of Folic Acid, ACS Omega, (2019).

[49] A. Hebeish, M. Hashem, M.A. El-Hady, S. Sharaf, Development of CMC hydrogels loaded with silver nano-particles for medical applications, Carbohydrate polymers, 92 (2013) 407-413.

[50] N.M.H. Mohamed, N.N.E. Hassan, An investigation into the physical and functional properties and sew ability of Faux leather, Int. J. Des, 5 (2011) 375-383.

[51] Y. Li, W. Wu, F. Lin, A. Xiang, The interaction between poly (vinyl alcohol) and low-molar-mass poly (ethylene oxide), Journal of Applied Polymer Science, 126 (2012) 162-168.

[52] W. Silva, N. Ferreira, J. Soares, R. Da Silva, M. Macêdo, Investigation of structural and magnetic properties of nanocrystalline Mn-doped SrFe12O19 prepared by proteic sol–gel process, Journal of Magnetism and Magnetic Materials, 395 (2015) 263-270.

[53] S.B. Şentürk, D. Kahraman, C. Alkan, İ. Gökçe, Biodegradable PEG/cellulose, PEG/agarose and PEG/chitosan blends as shape stabilized phase change materials for latent heat energy storage, Carbohydrate Polymers, 84 (2011) 141-144.

[54] N.E. Kochkina, O.A. Butikova, Effect of fibrous TiO2 filler on the structural, mechanical, barrier and optical characteristics of biodegradable maize starch/PVA composite films, International journal of biological macromolecules, 139 (2019) 431-439.

[55] M. Nisar, P.S. Thue, C.A. Heck, J.S. Cuaila, J. Geshev, E.C. Lima, M.M. Jacobi, G.B. Galland, Synthesis of polyethylene/nickel–carbon stimuli-responsive material under magnetic field at room temperature: Effect of the filler on the properties, European Polymer Journal, 99 (2018) 378-383.

[56] M.L. Di Lorenzo, M. Cocca, M. Avella, G. Gentile, D. Gutierrez, M. Della Pirriera, E. Torralba-Calleja, M. Kennedy, H. Ahmed, J. Doran, Down shifting in poly (vinyl alcohol) gels doped with terbium complex, Journal of colloid and interface science, 477 (2016) 34-39.

[57] K. Jlassi, S. Chandran, M. Mičušik, M. Benna-Zayani, Y. Yagci, S. Thomas, M.M. Chehimi, Poly (glycidyl methacrylate)-grafted clay nanofiller for highly transparent and mechanically robust epoxy composites, European Polymer Journal, 72 (2015) 89-101.

[58] A. Youssef, M.A. El-Aziz, E.S.A. El-Sayed, M. Moussa, G. Turky, S. Kamel, Rational design and electrical study of conducting bionanocomposites hydrogel based on chitosan and silver nanoparticles, International journal of biological macromolecules, 140 (2019) 886-894.

[59] N. Masood, R. Ahmed, M. Tariq, Z. Ahmed, M.S. Masoud, I. Ali, R. Asghar, A. Andleeb, A. Hasan, Silver nanoparticle impregnated chitosan-PEG hydrogel enhances wound healing in diabetes induced rabbits, International journal of pharmaceutics, 559 (2019) 23-36.

[60] A.A. Oun, J.-W. Rhim, Carrageenan-based hydrogels and films: Effect of ZnO and CuO nanoparticles on the physical, mechanical, and antimicrobial properties, Food Hydrocolloids, 67 (2017) 45-53.

[61] M.A. Scorciapino, R. Sanna, A. Ardu, F. Orrù, M. Casu, A. Musinu, C. Cannas, Core–shell nano-architectures: The incorporation mechanism of hydrophobic nanoparticles into the aqueous core of a microemulsion, Journal of colloid and interface science, 407 (2013) 67-75.

[62] Y. Huang, Y. Li, Y. Wang, Magnetic and electromagnetic properties of Pr doped strontium ferrite/polyaniline composite film, Journal of Magnetism and Magnetic Materials, 368 (2014) 133-138.

[63] Y. Li, Y. Huang, S. Qi, L. Niu, Y. Zhang, Y. Wu, Preparation, magnetic and electromagnetic properties of polyaniline/strontium ferrite/multiwalled carbon nanotubes composite, Applied Surface Science, 258 (2012) 3659-3666.

[64] X. Liang, C. Ma, X. Yan, H. Zeng, D.J. McClements, X. Liu, F. Liu, Structure, rheology and functionality of whey protein emulsion gels: Effects of double cross-linking with transglutaminase and calcium, Food Hydrocolloids, (2019) 105569.

[65] A.M. Al-Enizi, T. Ahamad, A.B. Al-hajji, J. Ahmed, A.A. Chaudhary, S.M. Alshehri, Cellulose gum and copper nanoparticles based hydrogel as antimicrobial agents against urinary tract infection (UTI) pathogens, International journal of biological macromolecules, 109 (2018) 803-809.

[66] H. Bian, L. Jiao, R. Wang, X. Wang, W. Zhu, H. Dai, Lignin nanoparticles as nano-spacers for tuning the viscoelasticity of cellulose nanofibril reinforced polyvinyl alcohol-borax hydrogel, European Polymer Journal, 107 (2018) 267-274.

1

Figure Captions

Figure 1: Optical images of air-dried (a-d) and freeze-dried (e-h) magnetic hydrogels: PVA/CMC (control) (a and e), PVA/CMC/MG 8 (b and f), PVA/CMC/MG 10 (c and g) and PVA/CMC/MG 12 (d and h), respectively.

Figure 2: (a) FTIR spectra of different hydrogels (i) PVA; (ii) CMC; (iii) PVA/CMC (control); (iv) PVA/CMC/MG8; (v) PVA/CMC/MG10 and (vi) PVA/CMC/MG12 hydrogels; (b) X-ray diffraction patterns of (i) SrFe magnetic nanoparticles, (ii) PVA; (iii) CMC; (iv) PVA/CMC (control); (v) PVA/CMC/MG8; (vi) PVA/CMC/MG10 and (vii) PVA/CMC/MG12 hydrogels.

Figure 3: Scanning electron micrographs of cross-sectional view (a-d) and surface morphologies (a′-d′) of (a and a′) PVA/CMC (control); (b and b′) PVA/CMC/MG8; (c and c′) PVA/CMC/MG10 and (d and d′) PVA/CMC/MG12 hydrogels.

Figure 4: Stress vs. strain curves for various PVA/CMC hydrogels with different concentration of magnetic nanofiller loadings.

Figure 5: (a) TGA (b) DTG and (c) DSC curves for PVA/CMC (control) and PVA/CMC/MG magnetic hydrogels.

Figure 6: Variation in thermomechanical properties, (a) storage modulus (E′) and (b) loss factor (tan δ) as a function of temperature with increasing MG loading (wt%).

Figure 7: (a) Variation in swelling behavior as a function of time and (b) images of contact angles with water and diiodomethane for PVA/CMC (control) and PVA/CMC/MG magnetic hydrogels.

Figure 8: (a) Magnetization curves for PVA/CMC/MG magnetic hydrogels, inset: Magnetization curves of strontium ferrite nanoparticles, (b) Effect of angular frequency (α) at 1% strain on (a) storage modulus (G′), (b) loss modulus (G′′) and (c) complex viscosity (η^*) for PVA/CMC/MG magnetic hydrogels.

Scheme 1: Schematic representation of the preparation of PVA/CMC/MG hydrogels.

Highlights

- PVA/CMC hydrogels containing strontium ferrite nanoparticles were synthesized.
- Moist heat treatment method was used to physically crosslink the hydrogels.
- Magnetic fillers improve the mechanical and thermal properties.
- Magnetic hydrogels have high flexibility and film forming ability
- PVA/CMC/MG hydrogels are biodegradable, sweat absorbing, odor-resistant and comfortable as compared to plastic based magnetic diabetic insoles.

Table 1: Sample codes and composition of hydrogels used in this research work.

Sample code	PVA (g)	CMC (g)	PEG (g)	Agar (g)	Glycerin (g)	SrFe (g)	Water (mL)
PVA/CMC (control)	1	1	3	1	3	0	100
PVA/CMC/MG 8	1	1	3	1	3	0.8	100
PVA/CMC/MG 10	1	1	3	1	3	1.0	100
PVA/CMC/MG 12	1	1	3	1	3	1.2	100

Table 2: Summary of mechanical properties of the PVA/CMC hydrogel samples.

Hydrogels	Young's Modulus, E (MPa)	Ultimate Tensile Strength, σ (N/mm^2)	Elongation at Break, ε (%)	Stress at Break (MPa)
PVA/CMC (Control)	17.2±0.9	1.6±0.1	32.0±2.5	1.5±0.1
PVA/CMC/MG 8	8.5±3.6	1.3±0.1	42.5±1.0	1.3±0.1
PVA/CMC/MG 10	13.3±3.3	1.9±0.4	45.0±4.0	1.6±0.1
PVA/CMC/MG 12	11.8±1.7	1.8±0.1	49.0±1.0	1.7±0.1

Table 3: contact angle and surface free energy (SFE) values for control and magnetic hydrogels. (DIM: diiodomethane)

Hydrogels	**Contact angle**		**Surface free energy (γ_S), mN/m**	**Polar (γ_S)**	**disperse (γ_S^D)**
	water	**DIM**			
PVA/CMC (control)	25.2	45.4	69.8	36.8	33.0
PVA/CMC/MG 8	30.9	44.4	67.3	37.3	30.0
PVA/CMC/MG 10	27.9	50.4	67.5	34.03	33.5
PVA/CMC/MG 12	29.9	41.5	68.4	38.8	29.6

Table 4: Magnetic properties of strontium ferrite nanoparticles and fabricated PVA/CMC/MG magnetic hydrogels.

Properties	**SrFe**	**CMC/PVA/MG 8**	**CMC/PVA/MG 10**	**CMC/PVA/MG 12**
BH_{max}, Goe	8.9×10^5	345.2 ± 47.4	512.9 ± 60.3	442.7 ± 23.7
B_r, G	2096.6	37.6 ± 3.0	45.5 ± 2.7	42.7 ± 1.4
Coercivity, H_c, Oe	4592.1	4630.9 ± 2.2	4658 ± 20.3	4633.8 ± 19.6
Saturation magnetization (M_s), emu/g	51.5	3.6 ± 0.2	4.3 ± 0.2	4.0 ± 0.2
Remanent magnetization (M_r), emu/g	32.2	2.2 ± 0.1	2.7 ± 0.1	2.5 ± 0.1

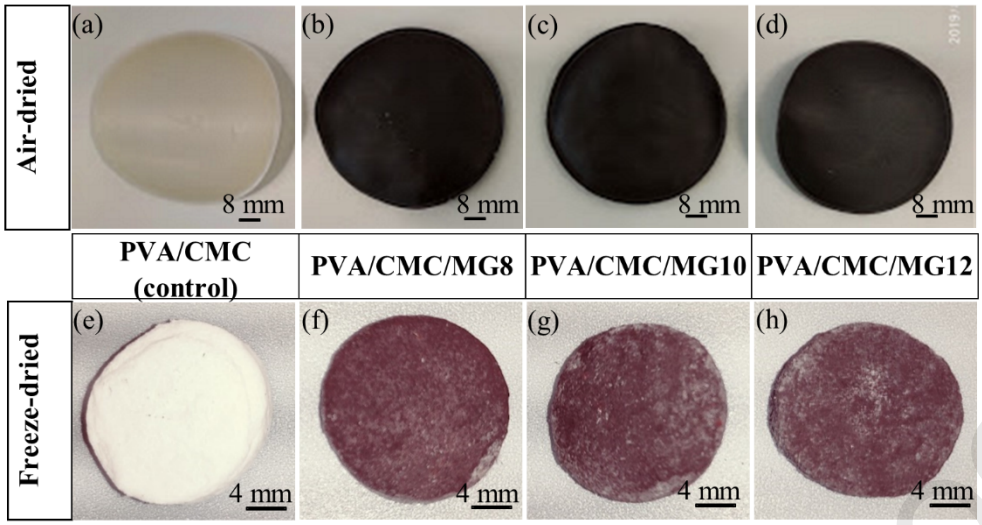

1

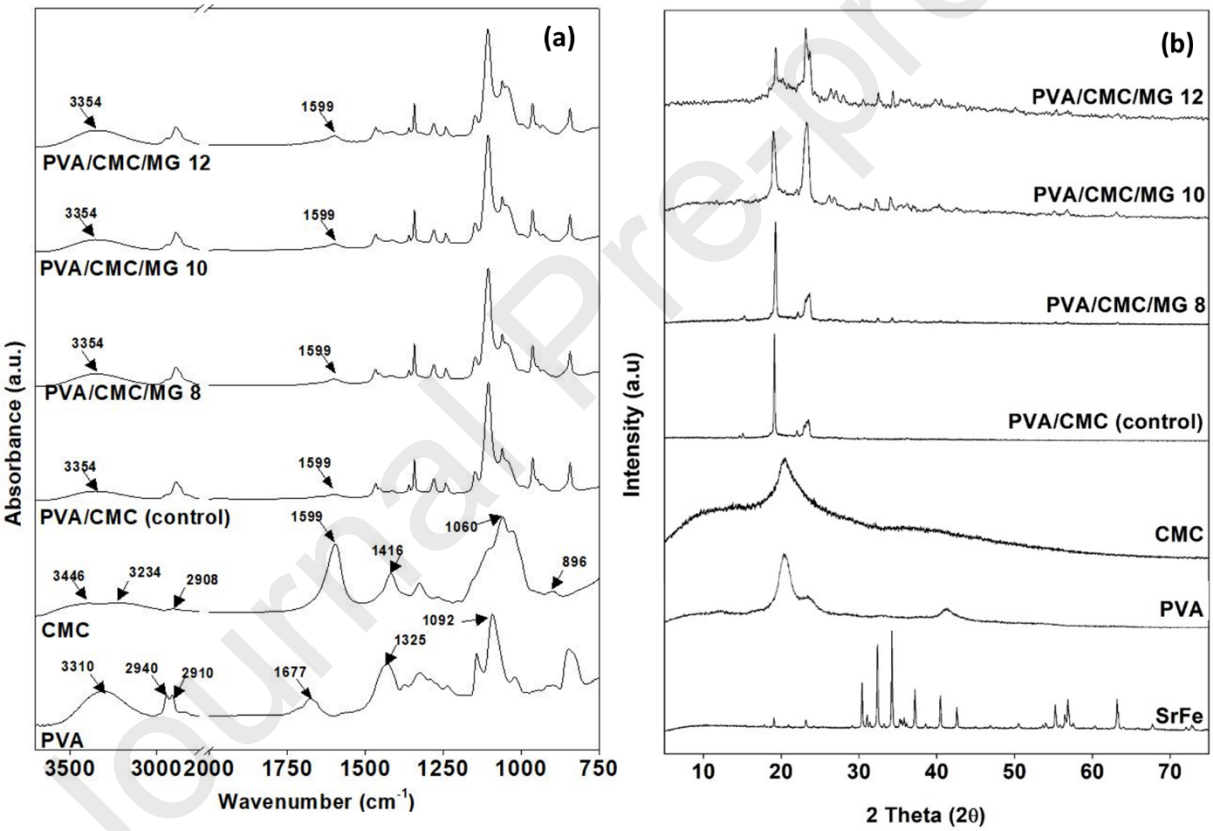

2

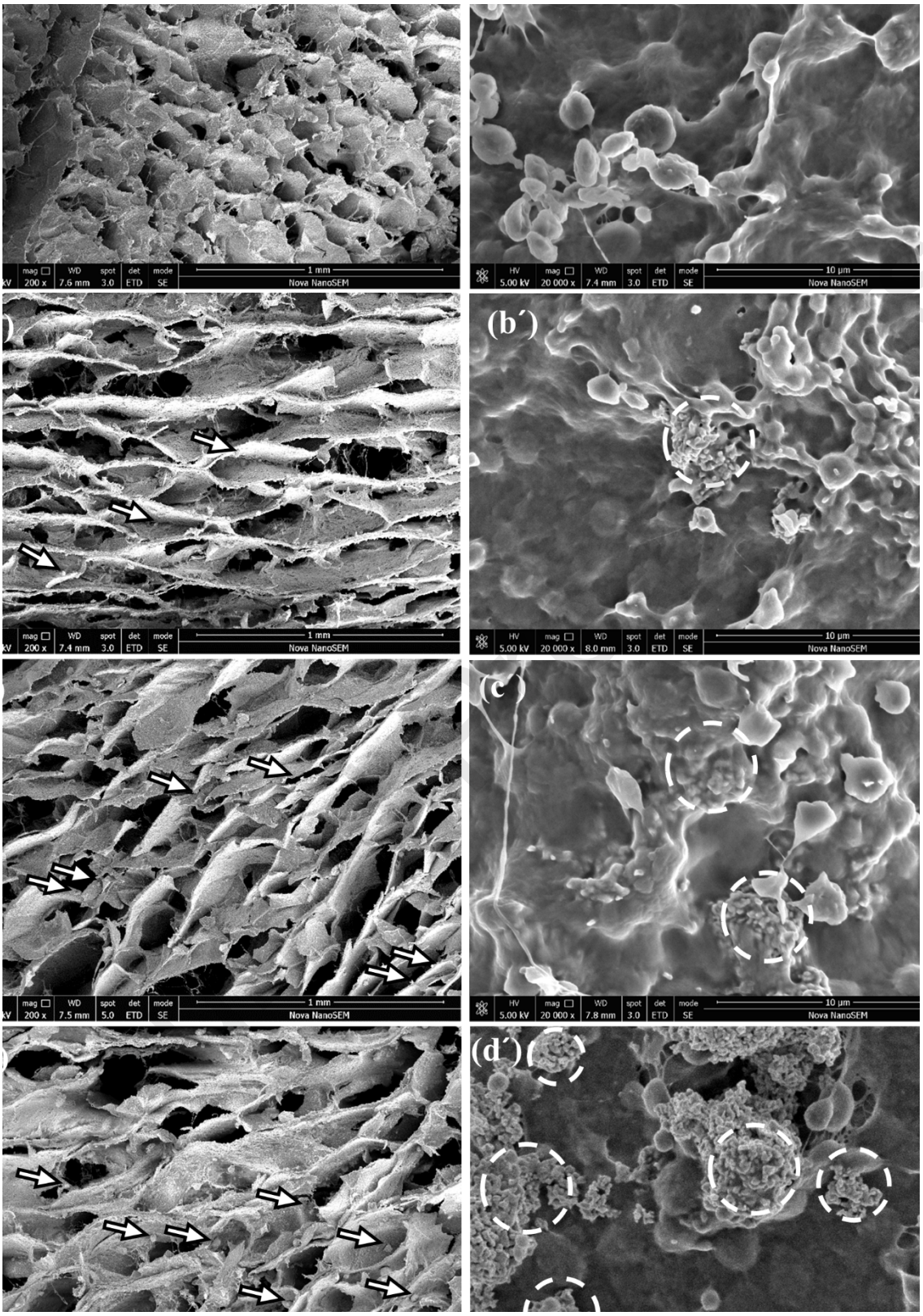
(b´)
(c´)
(d´)
mag 200 x WD 7.6 mm spot 3.0 det ETD mode SE 1 mm Nova NanoSEM
HV 5.00 kV mag 20 000 x WD 7.4 mm spot 3.0 det ETD mode SE 10 µm Nova NanoSEM
mag 200 x WD 7.4 mm spot 3.0 det ETD mode SE 1 mm Nova NanoSEM
HV 5.00 kV mag 20 000 x WD 8.0 mm spot 3.0 det ETD mode SE 10 µm Nova NanoSEM
mag 200 x WD 7.5 mm spot 5.0 det ETD mode SE 1 mm Nova NanoSEM
HV 5.00 kV mag 20 000 x WD 7.8 mm spot 3.0 det ETD mode SE 10 µm Nova NanoSEM

1

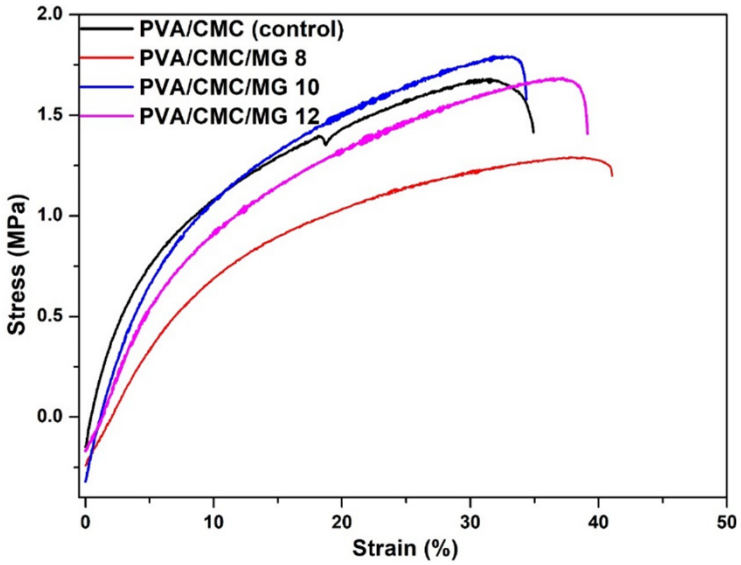

1

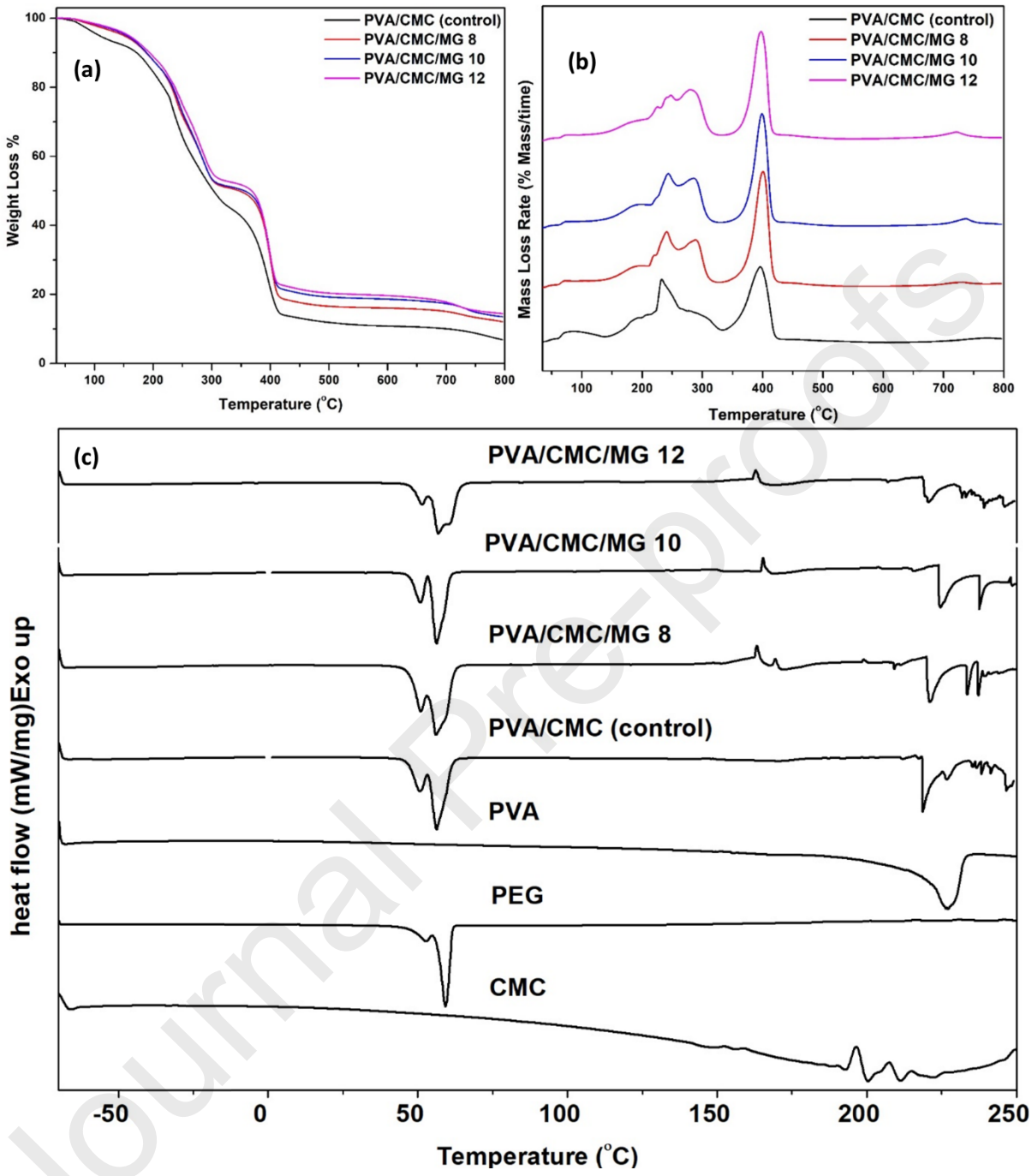

1

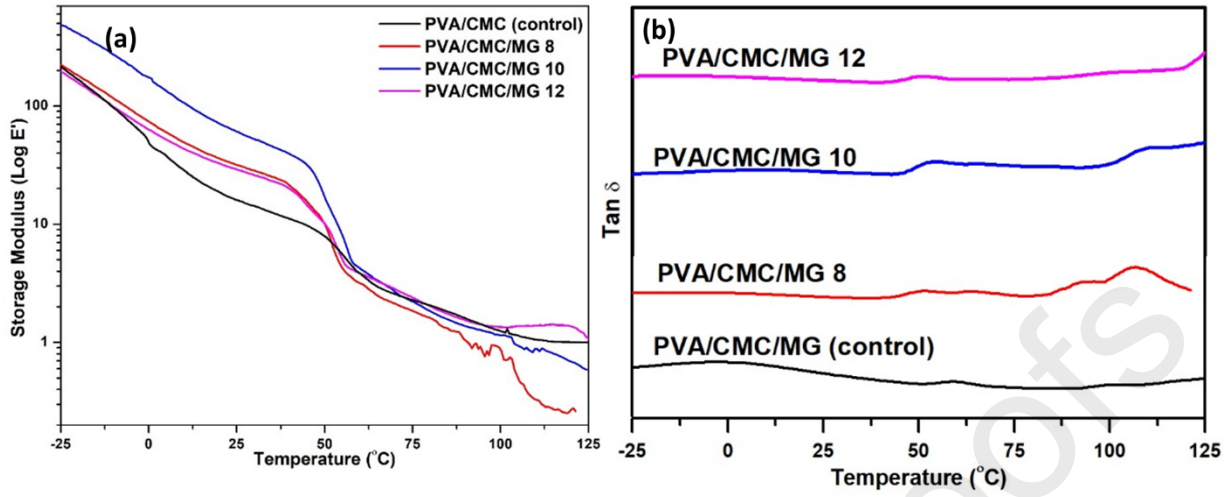

1

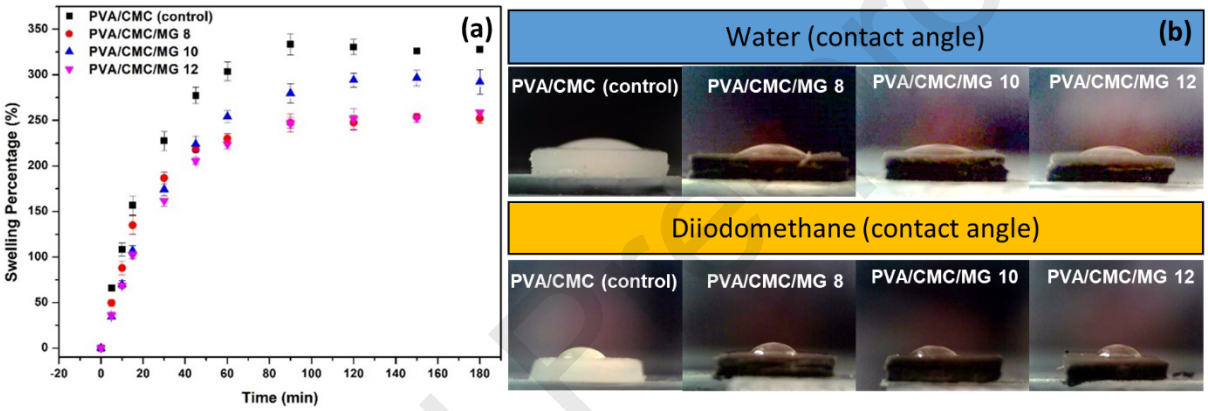

2

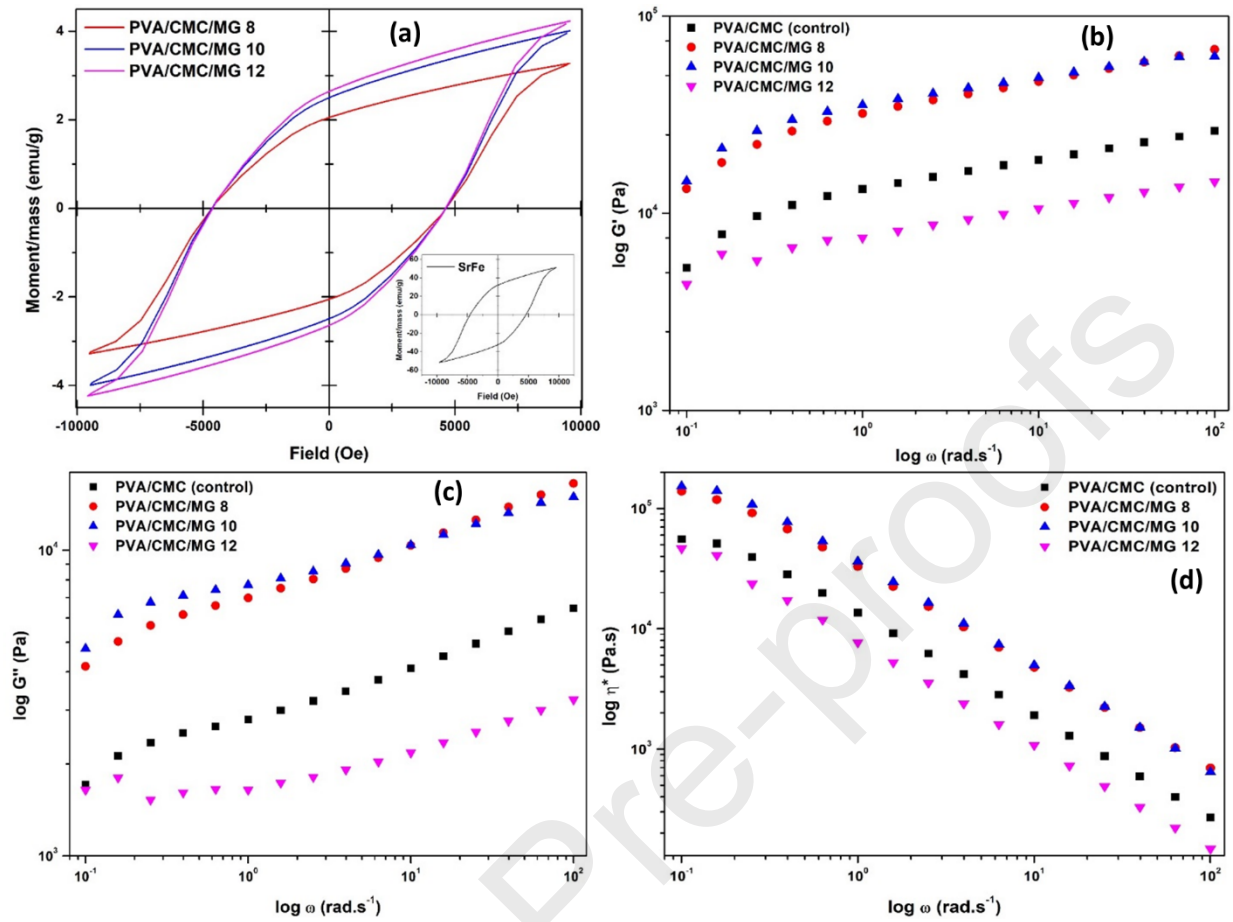

1

2

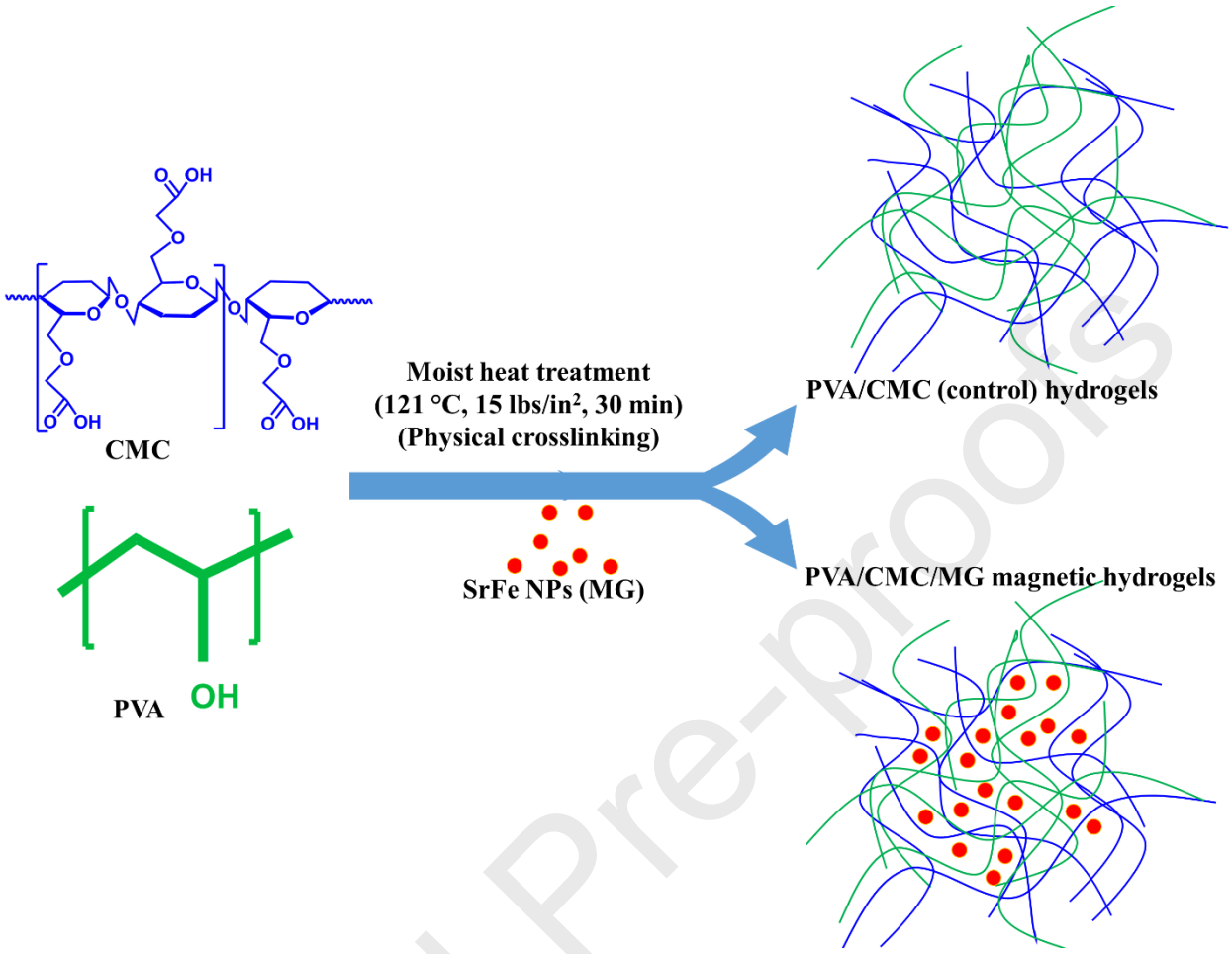

1